Physico-chemical, antimicrobial and antioxidant properties of gelatin-chitosan based films loaded with nanoemulsions encapsulating active compounds

Luis J. Pérez-Córdoba[a,b]*, Ian T. Norton[b], Hannah K. Batchelor[c], Konstantinos Gkatzionis[b], Fotios Spyropoulos[b], Paulo J.A. Sobral[a]

[a] Department of Food Engineering, Faculty of Animal Science and Food Engineering, University of São Paulo, Pirassununga 13635-900, São Paulo, Brazil. *E-mail: luchop283@usp.br.

[b] School of Chemical Engineering, University of Birmingham, Edgbaston, Birmingham B15 2TT, UK

[c] Pharmacy School, University of Birmingham, Edgbaston, Birmingham B15 2TT, UK

Abstract

The aim of this research was to develop and characterize gelatin-chitosan (4:1) based films that incorporate nanoemulsions loaded with a range of active compounds; N_1: canola oil; N_2: α-tocopherol/cinnamaldehyde; N_3: α-tocopherol/garlic oil; or N_4: a-tocopherol/cinnamaldehyde and garlic oil. Nanoemulsions were prepared in a microfluidizer with pressures ranging from 69 to 100 MPa, and 3 processing cycles. Films were produced by the casting method incorporating 5g $N_{1,2,3,4}$/100 g biopolymers and using glycerol as a plasticizer, and subsequently characterized in terms of their physico-chemical, antimicrobial and antioxidant properties. No differences ($p>0.05$) were observed for all films in terms of moisture content (18% w/w), and thermal properties. The films' solubility in water and light transmission at 280 nm were considerably reduced as compared to the control, N_1 (15% and 60% respectively) because of the nanoemulsion incorporation. The film loaded with N_1 showed the greatest ($p<0.05$) opacity, elongation at break and stiffness reduction, and was the roughest, whilst the lowest tensile strength and ability to swell were attained by films loaded with N_3 and N_4, respectively. DSC and X-ray analyses suggested compatibility among the biopolymeric-blend, and a good distribution of nanodroplets embedded into the matrix was confirmed by AFM and SEM analyses. Films loaded with nanoencapsulated active compounds (NAC) were very effective against *Pseudomonas aeruginosa*, and also showed high antioxidant activity. Overall, the present study offers clear evidence that these active-loaded films have the potential to be utilized as packaging material for enhancing food shelf life.

Keywords: biopolymer, active films, emulsion, α-tocopherol, cinnamaldehyde, garlic oil.

Chemical compounds studied in this article:

Cinnamaldehyde (PubChem CID: 637511); alpha-tocopherol (PubChem CID: 14985); Garlic oil (PubChem CID: 6850738); Tween 20 (PubChem CID: 443314); Span 60 (PubChem CID: 14928); Chitosan (21896651); Acetic acid (PubChem CID: 176); Glycerol (PubChem CID: 753); 2,2'-azino-

bis(3-ethylbenzothiazoline-6-sulphonic acid) (PubChem CID: 16240279); 1,1-Diphenyl-2-picrylhydrazyl (PubChem CID: 2735032).

1. Introduction

The development of biodegradable packaging has been the focus of recent research, as an alternative to plastic material derived from petroleum, which due to their poor biodegradation generate a massive accumulation of plastic waste in the environment (Arancibia, Giménez, López-Caballero, Gómez-Guillén, & Montero, 2014; Rubilar et al., 2013). Films based on biopolymers do not have the same physical properties as synthetic plastics, but they present a promising application because they generally are from renewable sources, non-toxic, biodegradable, biocompatible, and sometimes could become edible material (Chen et al., 2016; Kurek, Galus, & Debeaufort, 2014; Pérez-Córdoba & Sobral, 2017). Furthermore, these films are excellent vehicles for incorporating a wide variety of active agents, such as antioxidant and antimicrobial compounds, and thus, these biodegradable materials can be used for active packaging (Abdollahi, Rezaei, & Farzi, 2012; Rhim & Ng, 2007).

According to Gennadios, McHugh, Weller, & Krochta (1994), gelatin (G) was one of the first materials used as a carrier of bioactive components. Gelatin is a protein obtained by hydrolyses of the collagen from bones and skin via exposure to acidic (type-A) or alkaline (type-B) pre-treatment conditions (Gómez-Guillén et al., 2009). Gelatin has excellent film-forming properties and can generally form films with good mechanical characteristics that also act as barriers to oxygen, carbon dioxide, and volatile compounds (Tongnuanchan, Benjakul, & Prodpran, 2012); they form however a relatively poor barrier to moisture mainly due to the hydrophilic nature of the gelatin molecules (Ahmad et al., 2012). Moreover, gelatin has the ability to blend well with others biopolymers, such as chitosan (Bonilla & Sobral, 2016; Pérez-Córdoba & Sobral, 2017).

Chitosan (Ch) is a linear polysaccharide consisting of β-(1–4)-2-acetamido-D-glucose and β-(1–4)-2-amino-D-glucose units, derived from chitin through deacetylation in alkaline media, and it is the second most abundant polysaccharide found in nature, after cellulose (Baron, Pérez, Salcedo, Pérez-Córdoba, & Sobral, 2017; Elsabee & Abdou, 2013). Similar to gelatin, chitosan has excellent film-forming properties and offers great potential as the basis for active packaging material due to its intrinsic antimicrobial activity (Kanatt, Rao, Chawla, & Sharma, 2012). Blending chitosan with gelatin can produce films with improved properties, showing antimicrobial or antioxidant activity due to the presence of chitosan, or following the incorporation of hydrophilic bioactive agents (Benbettaïeb, Kurek, Bornaz, & Debeaufort, 2014; Bonilla & Sobral, 2016; Hosseini, Rezaei, Zandi, & Ghavi, 2013; Jridi et al., 2014; Pereda, Ponce, Marcovich, Ruseckaite, & Martucci, 2011; Rivero, García, & Pinotti, 2009).

More recently, a number of studies have reported biopolymer films loaded with lipophilic compounds that are dispersed within the hydrophilic film structure as nanodroplets (nanoemulsions) (Acevedo-Fani, Salvia-Trujillo, Rojas-Graü, & Martín-Belloso, 2015; Alexandre, Lourenço, Quinta

Bittante, Moraes, & Sobral, 2016; Chen et al., 2016; Otoni, Avena-Bustillos, Olsen, Bilbao-Sáinz, & McHugh, 2016; Sasaki, Mattoso, & de Moura, 2016). In parallel to these studies, other works have focused on the encapsulation of essential oils within a nanoemulsion microstructure (Sasaki et al., 2016), flavonoids, such as rutin (Dammak & Sobral, 2017), curcumin (Sari et al., 2014) and other compounds like α-tocopherol (Cheong, Tan, Man, & Misran, 2008; Yang & McClements, 2013), cinnamaldehyde (Donsì, Annunziata, Vincensi, & Ferrari, 2012) or garlic oil (Wang, Cao, Sun, & Wang, 2011). Potential applications of nanoemulsions for the encapsulation of bioactive components, either as a viable and efficient approach to increase their physical stability or in order to minimize their potentially detrimental sensorial effects, have been well documented within the food sciences research arena (Donsì, Annunziata, Sessa, & Ferrari, 2011; Fathi, Mozafari, & Mohebbi, 2012).

Among such bioactive compounds recently studied, α-tocopherol (α-t), cinnamaldehyde (Cin), and garlic oil (GO) have been shown to exhibit a wide range of biological effects including antimicrobial and/or antioxidant properties (Donsì et al., 2012; Wang et al., 2011; Yang & McClements, 2013). α-tocopherol is an isomer and the most naturally abundant and biologically active form of vitamin E in humans (Yang & McClements, 2013) and it has been shown to have high antioxidant activity in both biological and food systems (Saberi, Fang, & McClements, 2013). Cinnamaldehyde is a hydrophobic aromatic compound with a benzene ring and an aldehyde group. It is the main active component of cinnamon oil (Chen et al., 2016) and it has been shown to be active against a broad range of foodborne pathogens bacteria, fungi and viruses (Wei, Xiong, Jiang, Zhang, & Wen Ye, 2011). Garlic oil is an essential oil extracted from garlic bulbs, which contains a range of compounds; mainly diallyl disulfide (60%), diallyl trisulfide (20%), allyl propyl disulfide (16%), a small quantity of disulfide and possibly diallyl polysulfide (Pranoto, Rakshit, & Salokhe, 2005). It is also used as a food preservative and it has been shown to inhibit the growth of a wide range of pathogens and spoilage microorganisms, including bacteria, mold, fungi, parasites and viruses (Sung, Sin, Tee, Bee, & Rahmat, 2014). All three of these active compounds have been categorized as safe (GRAS) for use in food by the US Food and Drug Administration (FDA) (Chen et al., 2016; Wei et al., 2011) and have been independently used as active additives within a range of packaging formulations (Noronha, De Carvalho, Lino, & Barreto, 2014; Otoni et al., 2016; Pranoto et al., 2005). However, they are poorly soluble in water and as such extremely difficult to incorporate within film formulations, which are usually hydrophilic/aqueous systems (Alexandre et al., 2016).

The present study reports on a microstructural approach that involves the encapsulation of active compounds within oil-in-water (O/W) nanoemulsions, before incorporating these into a biopolymer film formulation, in order to facilitate dispersion of the bioactive species into the biopolymer matrix (Chen et al., 2016). To the best of the authors' knowledge, the joint incorporation of nanoencapsulated active compounds (NAC), such as α-t, plus Cin and/or GO, within gelatin-chitosan (G-Ch) based films, in order to improve the films' physicochemical, antimicrobial and antioxidant properties, has not been previously reported. The objective of this work was to successfully produce G-

Ch based films loaded with O/W nanoemulsions containing the encapsulated α-t, and Cin and/or GO active compounds and then characterize these formulations in terms of moisture content, solubility in water, swelling, light transmission, opacity, crystallinity, mechanical and thermal properties, microstructure, as well as their antioxidant and antimicrobial activities, thus enabling future development and application of such composite systems as food packaging material.

2. Material and Methods

2.1 Material

Garlic oil (purity >99%), cinnamaldehyde (>95%), and α-tocopherol (>96%), Span 60, medium molecular weight chitosan (degree of deacetylation: 75–85% and viscosity: 200–800 cps), Trolox, TPTZ (2,4,6-tripyridyl-*s*-triazine), chloride acid, Iron trichloride, and ethanol were purchased from Sigma-Aldrich and Labsynth (São Paulo, Brazil). Pigskin gelatin (type A, bloom 260º and molecular weight ~5.2 x 10^4 Da) was supplied by GELNEX (Itá, SC, Brazil). Acetic acid, glycerol, Tween 20, DPPH (2,2-diphenyl-1-picrylhydrazyl), potassium persulfate, $ABTS^{\bullet+}$ [2,2'-azino-bis(3-ethylbenzothiazoline-6-sulphonic acid)], sodium bromide, sodium hydroxide, nutrient broth, and Mueller Hinton agar were obtained from Sigma-Aldrich (Dorset, England, UK). Canola oil was purchased from a local supermarket. Deionized Millipore water (Elix® 5UV, essential), tetracycline, and strains of bacteria *P. aeruginosa* (ATCC 15692) and *L. monocytogenes* (ATCC 35152) were provided by the microbiology laboratory at the School of Biochemical Engineering of the University of Birmingham.

2.2 Nanoemulsion preparation

The α-tocopherol and cinnamaldehyde and/or garlic oil were encapsulated in nanoemulsions using the microfluidization technique. Three oil-in-water (O/W) nanoemulsions containing a fixed amount of 3% (w/v) α-t/Cin (N_2), α-t/GO (N_3), or an equimolar mixture of α-t/Cin and GO (N_4) were prepared by firstly incorporating these active compounds into canola oil, using Span 60 (1.5 w/v) as the lipophilic emulsifier. This oil phase (10 % w/v) was then initially mixed with an aqueous phase containing water and Tween 20 (3.5% w/v) as the hydrophilic emulsifier in a 1:9 ratio using a magnetic stirrer (RH basic2, IKA, Germany) for 5 min at room temperature. Afterwards, a coarse emulsion was prepared using a high shear mixer (Silverson L5M, Buckinghamshire, UK) operating at 5000 rpm for 5 min. These coarse emulsions were analyzed by optical microscopy (DFC 450C, Leica, Germany). Nanoemulsions were obtained by passing the coarse emulsion through a microfluidizer (M-110S, Microfluidics, USA) at different pressures (69 – 100 MPa) and 3 processing cycles, selected after previous optimization (data not shown).

An O/W nanoemulsion with the same oil:aqueous phase (1:9) ratio, without active compounds, was prepared following the same procedure, and it was considered as a control (N_1). Samples were stored in amber glass containers at 4 ± 1°C and their stability was monitored over a period of 90 days.

147 The encapsulation efficiency (EE) of all active species within the nanoemulsions was calculated
148 immediately post-emulsification and after 90 days of storage (Equation 1).

149 $$EE = (AC_R/AC_I)x100 \quad (1)$$

150 where AC_R is the amount of active compound (α-t, Cin or GO) remaining within the droplets of the
151 nanoemulsion, determined as described below, and AC_I is the amount of active compound initially
152 added to the emulsion (Davidov-Pardo & McClements, 2015).

153 The amount of active compound (α-t, Cin or GO) remaining within the droplets of the
154 nanoemulsion was determined by using an UHPLC$^+$ (Dionex Ultimate 3000, Thermo scientific,
155 Germany). Analyses were carried out by diluting the sample in methanol to facilitate the α-tocopherol
156 and garlic oil (0.01% v/v) or cinnamaldehyde (0,003% v/v) detection. The diluted samples were
157 separated in a Phenomenex Luna 3a C18 column (150 x 4.6 mm, i.d. 3 μm) with an elution system of
158 methanol:acetonitrile:water (68:28:4) for α-tocopherol or methanol:acetonitrile:phosphoric acid (1%
159 v/v) (50:30:20) for cinnamaldehyde and garlic oil. The flow rate of the mobile phase solvents was 1
160 mL/min, the injection volume was 25 μL (α-t) or 10 μL (Cin and GO), and the detection wavelength
161 was set at 208, 285 and 210 nm, for α-t, Cin and GO respectively (Mao, Yang, Xu, Yuan, & Gao, 2010).

162 The nanoemulsions were characterized in terms of their mean particle size, polydispersity
163 index, and ζ-potential using a Zetasizer (Nanoseries, Malvern Instruments, UK), pH using a pHmeter
164 (SevenCompact, Mettler Toledo, Switzerland), flow behavior using a rheometer (Kinexus Pro$^+$,
165 Malvern Instruments, UK), and microstructure and morphology using atomic force microscopy (Ntegra
166 prima, NT-MDT Co., Russia). All measurements were performed at least in triplicate. These
167 characterized nanoemulsions (N_1, N_2, N_3, and N_4) were then incorporated within the fabricated G-Ch
168 based films.

169

170 **2.3 Film production**

171 Films were produced by blending G-Ch (4:1 ratio) using the casting technique. A film-forming
172 solution (FFS) (5 g biopolymer/100 g FFS), loaded with nanoemulsions encapsulating active
173 compounds (5 g/100 g biopolymer) and glycerol (30 g/100 g biopolymer) as the plasticizer, was used.
174 Gelatin and chitosan solutions loaded with nanoemulsions were prepared separately, then, the FFS was
175 mixed under stirring in a plate stirrer (SB162-3, Stuart, UK) for 10 min, and subsequently homogenized
176 using a high shear mixer (Silverson L5M, Buckinghamshire, UK) at 5000 rpm for 5 min. During
177 stirring, the pH was adjusted at 5.6 for complexation between chitosan and gelatin to take place; the
178 selected pH value is above the isoelectric point of gelatin (*Pi* = 4.5–5.2), where all the gelatin chains
179 are negatively charged, and below pH 6.2 in order to prevent chitosan precipitating out of solution
180 (Benbettaïeb et al., 2014). FFS was sonicated and degassed in a Sonicator (ultrasonic cleaner QS18,
181 Ultrawave, UK) at 50ºC for 10 min. Finally, FFS was poured into a plastic Petri dish (14 cm diameter)

and placed in a forced air oven (GPS/50/CLAD/250/HYD, Leader, UK) at 30 ± 0.5 °C for 24 h, in order to obtain the films.

After peeling from the petri dish, the films were conditioned inside desiccators containing a saturated solution of NaBr (relative humidity 58%) for 7 days, prior to the characterization of their physicochemical, antimicrobial, and antioxidant properties. For SEM and AFM analyses, the newly formed films were instead conditioned in silica gel (relative humidity 0 %) for the same period. Furthermore, two films were made using the same G-Ch blend (4:1). The first one was prepared without the incorporation of a nanoemulsion (N_0), while the second one was loaded with a control nanoemulsion (N_1) described in section 2.2. Both films were formed using glycerol as a plasticizer and they were produced and conditioned as described above; hereinafter referred to as control 1 and control 2 films, respectively.

2.4 Film Characterization

2.4.1 Thickness

A digital micrometer (AK9635D, Sealey, UK) was used to measure the film thickness to the nearest 0.001 mm at 10 random positions on the surface of each film produced (Barón et al. 2017).

2.4.2 Moisture content

Moisture content (MC) was determined by cutting film samples into discs (20 mm in diameter) and measuring the reduction in the mass of a minimum of 3 discs (from each film) following oven drying (GPS/50/CLAD/250/HYD, Leader, UK) at 105 °C for 24 h. The results were expressed as g of water/100 g of wet material (Barón et al. 2017). Measurements were performed in triplicate.

2.4.3 Solubility in water and swelling

For solubility in water (SW) and swelling (S) measurements, film samples were cut in discs (20 mm in diameter), weighed, and immersed in 50 mL of distilled water under stirring in a shaker (Incu-Shake MIDI, SciQuip, UK) at 60 rpm and at room temperature for 24 h. Film samples were then removed from the solution, re-weighed, and dried in an oven at 105°C for 24 h to determine their final dry matter. These values were then used to calculate SW and S, expressed as g of solubilized mass/100 g of dried material and g of gained water/g of dried material, respectively (Gontard et al. 1994). All measurements were carried out in triplicate.

2.4.4 Mechanical properties

Tensile strength (TS), elongation at break (EB), and elastic modulus (EM) were measured according to the ASTMD 882/12 standard method (2001). Samples were cut into 15 mm x 100 mm strips, and tested using a texture analyzer (TA.XT2i, Stable Micro System, UK) with grip separation of 50 mm and speed rate of 1 mm/s until breaking. TS and EB were obtained directly from the stress *vs.*

strain curves, which are produced from the force–deformation data, and the EM was determined as the angular coefficient in the linear part of the curve using the Exponent Lite v.4.0.13.0 software (Stable Micro System, UK) (Baron et al., 2017). Data were collected for at least 10 sample strips from each film.

2.4.5 Light transmission and transparency

Light transmission of films against ultraviolet and visible light was determined in transmittance mode at selected wavelengths (200 to 800 nm) using a UV-VIS spectrophotometer (Orion AquaMate 8000, Thermo Scientific, Germany), according to the procedure described by Bonilla & Sobral (2016).

The transparency value for each film was calculated using Equation 2.

$$\text{Transparency value} = (-\log T_{600})/x \quad (2)$$

where T_{600} is the fractional transmittance at 600 nm, and x is the film thickness (mm). The higher transparency value represents the lower transparency of films (Ahmad et al., 2012). Five samples of each film were used for transmittance measurements.

2.4.6 X-ray diffraction (XRD)

XRD was used to determine the film's crystallinity. Analyses were carried out using an X-ray diffractometer (Miniflex600, Rigaku, Japan) with Cu as the source. Samples were cut in squares of 20 mm x 20 mm and placed on a glass plate, which was placed inside the chamber of the equipment. Measurements were recorded in triplicate at room temperature, 40 kV and 40 mA current, in the region of 2θ from 8º to 70º (with a constant speed of 1º min^{-1}) using the Miniflex Guidance software (Rigaku, Japan) (Chen et al., 2016).

2.4.7 Differential scanning calorimetry (DSC)

Thermal properties of the films were determined using a differential scanning calorimeter (DSC TA2010, TA Instruments, USA), controlled by a TA5000 system (TA Instruments, USA) and a quench cooling accessory. Approximately 10 mg (±0.01 mg) of sample were weighed in a precision balance (AP 2500 Analytical Plus, Ohaus, Switzerland), were conditioned in a hermetically sealed aluminum pan and heated in double run at 5ºC/min from -150 to 150 ºC in an inert atmosphere (45 ml/min of N_2). An empty pan was used as the control. The results were analyzed using the instrument's software (V1.7F, TA Instruments, USA) in order to determine the glass transition temperature (Tg), in the first and second scan, as well as the melting temperature (Tm) and enthalpy (ΔHm) of the sol-gel transition (Alexandre et al., 2016; Sobral, Menegalli, Hubinger, & Roques, 2001). DSC measurements were performed in triplicate.

255 **2.4.8 Atomic force microscopy (AFM)**

256 AFM analyses were performed according to Ma et al. (2012), using the atomic force microscope
257 (Topview optics™ Nanowizard, JPK Instruments, Germany) equipped with a DP17/GP/NAl
258 (μMASCH) tip and operated in contact mode. Samples (2 cm × 2 cm) from each film were pasted on a
259 glass slice using a double-sided adhesive tape. AFM images (with a scan size of 10 μm × 10 μm) were
260 collected from the air side of the films at a fixed scan rate of 0.7 – 0.8 Hz. The surface roughness of the
261 films was calculated based on the root mean square (RMS) deviation from the average height of peaks
262 after subtracting the background using the JPK-SPM and JPK Data processing software (JPK,
263 Germany) (Ma et al., 2012).
264
265 **2.4.9 Scanning electron microscopy (SEM)**

266 Film microstructures were studied using an environmental scanning electron microscope (FEG-
267 ESEM XL30, Phillips, Japan). Film samples were fixed on the support using double-sided adhesive
268 tape and initially coated with Platinum in a Sputter coater (SC7640, Quorum Technologies, UK) to
269 allow better observation of film surface and cross section. Micrographs of the films' surfaces and cross-
270 sections were taken in triplicate at random positions on the films, at 10 kV and a magnification of 1000x.
271 For cross-sectional analysis, samples were cryo-fractured after immersion in liquid nitrogen (Kurek et
272 al., 2014).
273
274 **2.4.10 Antimicrobial activity**

275 The antimicrobial activity of the films was assessed against *Pseudomonas aeruginosa* ATCC
276 15692 and *Listeria monocytogenes* ATCC 35152 by the agar diffusion method based on the guidelines
277 of the Clinical and Laboratory Standards Institute (CLSI, 2006) with slight modifications (Wayne,
278 2006). Microbial cultures were grown overnight in nutrient broth (Sigma Aldrich, England, UK) at 37
279 ºC and 150 rpm. The cells were harvested by centrifugation at 2000 rpm for 10 min and washed in
280 sterile phosphate buffer saline (pH 7.2) twice (Kadri, Devanthi, Overton, & Gkatzionis, 2017). Inocula
281 with a turbidity equivalent to a McFarland 0.5 standard were prepared (10^8 cfu/mL), then diluted to a
282 final concentration of 10^5 cfu/mL into Mueller Hinton agar (Merck, UK) and poured into petri plates
283 after mixing (Kavoosi, Rahmatollahi, Mohammad Mahdi Dadfar, & Mohammadi Purfard, 2014). After
284 solidification, discs (diameter 20 mm) of films containing the nanoemulsions N_1, N_2, N_3 and N_4 (or not,
285 N_0), were placed in plicate on the medium, and the plates were incubated at 37 ºC for 24 h. The area of
286 the whole zone was calculated, then subtracted from the film disc area, and this difference in area was
287 reported as the zone of inhibition (Seydim & Sarikus, 2006).
288
289 **2.4.11 Determination of antioxidant activity**

290 The films' antioxidant activity was measured using the 2,2'-azino-bis(3-ethylbenzothiazoline-
291 6-sulphonic acid) ($ABTS^{\bullet+}$) and 1,1-diphenyl-2-picrylhydrazyl ($DPPH^{\bullet}$) free radical scavenging

methods, and the ferric reducing ability of plasma (FRAP) assay, as described by Re et al. (1999), Brand-Williams, Cuvelier, & Berset (1995) and Ferreira, Nunes, Castro, Ferreira, & Coimbra (2014), respectively. For $ABTS^{\bullet+}$ and $DPPH^{\bullet}$ analyses, 0.1 g samples from each film were immersed into 10 ml of a hydroalcoholic mixture (1:1) and kept under agitation overnight at 80 rpm and 20ºC to encourage the extraction of the encapsulated compounds. All antioxidant analyses were performed in triplicate.

2.4.11.1 $ABTS^{\bullet+}$ method.

A solution containing $ABTS^{\bullet+}$ radical (7 mM) and potassium persulfate (2.45 mM) was initially mixed (1:0.5) and kept in the dark for 16 h. Subsequently, an aliquot of this solution was diluted with ethanol in order to prepare the $ABTS^{\bullet+}$ working solution with an absorbance value of 0.70 ± 0.02, as measured using a UV-Vis spectrophotometer at 734 nm. An aliquot (100 µL) of the solubilized and centrifuged (4000 rpm, 30 min) samples was added to the $ABTS^{\bullet+}$ working solution (900 µL), and the mixture was kept in the dark within 6 min (Bonilla & Sobral, 2016; Re et al., 1999). Antioxidant activity is calculated and expressed as Trolox equivalent TE (µmol/g dried film).

2.4.11.2 $DPPH^{\bullet}$ method.

A centrifuged (4000 rpm, 30 min) aliquot of the solubilized film (1.5 mL) was added to 1.5 mL of $DPPH^{\bullet}$ radical solution (60 µM), and it was kept in the dark for one hour. After this period, the absorbance was determined at 515 nm using a UV-Vis spectrophotometer (Brand-Williams et al., 1995). Antioxidant activity is calculated and expressed as Trolox equivalent TE (µmol/g dried film). Antioxidant activity is expressed as TE (µmol/g dried film).

2.4.11.3 FRAP assay

A solution of $FeCl_3$ (20 mM) was prepared in distilled water and TPTZ was prepared in 40 mM HCl. To prepare the FRAP reagent, 25 mL acetate buffer (0.3 M, pH 3.6) were mixed with 2.5 mL of TPTZ and 2.5 mL $FeCl_3$. Film samples of 50 mm x 50 mm (~ 2.5 mg) were placed in 3 mL of FRAP solution and 0.3 mL of distilled water for 24 h. Following this period, the absorbance of the film-containing solution was measured at 593 nm using a UV-Vis spectrophotometer. The absorbance of the FRAP solution (without the film) was also measured as a blank (Ferreira et al., 2014). Antioxidant activity is expressed as TE (µmol/g dried film).

2.5 Statistical analysis

Analysis of variance (ANOVA) was conducted using the Statgraphics® centurion XV (StatPoint, Inc., 2006) software. The obtained mean values were subjected to Duncan's multiple-range test, and in all cases, values with $p<0.05$ were considered to be significant.

3. Results and Discussion

3.1 Nanoemulsion characterization

3.1.1 Encapsulation efficiency

The results presented in Table 1 show that Cin and GO had higher EE than α-t during the encapsulation process and nanoemulsion storage. Nevertheless, all of them had a slight reduction in EE during storage. This loss could be associated with the high pressure and cycle number used in the nanoemulsion preparation or could be due to the partial volatility of those compounds, principally the Cin and GO. Furthermore, the harsh processing conditions, as well as the presence of heat, light, and oxygen during processing, could explain the active compound loss. These extreme conditions might have caused chemical degradation of α-tocopherol, resulting in a reduction of the quantified α-t concentration (Anarjan, Mirhosseini, Baharin, & Tan, 2011; Cheong et al., 2008). When comparing the EE for Cin or GO between N_2 or N_3 and N_4, which contain the three joint mixed compounds (Table 1), a clear reduction in the encapsulated compound quantified immediately post-emulsification and also a significant difference ($p<0.05$) between the EE values after 90 days of storage for both Cin and GO was seen. Hence, the fact that encapsulating three compounds instead of two, clearly affected their EE. On the other hand, the EE for α-t did not show significant difference ($p>0.05$) after post-emulsification regardless of the nanoemulsion. However the storage time had a significant ($p<0.05$) effect on the EE for this active compound in all nanoemulsions, which was expected due to the high sensitivity of this molecule (Nhan & Hoa, 2013).

Despite the obtained EE during the nanoemulsion preparation and the slight loss of the active compounds after 90 days under refrigeration, it was proven that the remaining NAC was sufficient to guarantee a very good antimicrobial and antioxidant properties for the prepared emulsions (data not shown.

3.1.2 Droplet size, polydispersity, ζ-potential and pH measurements

The nanoemulsions were also evaluated in terms of their physicochemical properties (Table 1). The control nanoemulsion (N_1) without encapsulated actives, presented the highest ($p<0.05$) droplet size, polydispersity index (PDI), ζ-potential, and pH values, among all tested formulations (Table 1). For nanoemulsions loaded with active compounds, mean particle size, PDI, and ζ-potential values remained between 111.0 and 130.0 nm, 0.14 – 0.20 and -12.0 to -16.0 mV, respectively, with all characteristics remaining unchanged over the 90 days storage (Table 1). All emulsions were found to possess droplet sizes within the desired nano-scale region with a monomodal size distribution (Figure 1). Moreover, it could be confirmed that those nanoemulsions presented an excellent physical stability across the 90-day storage at 4 ºC.

The nanoemulsions were also analyzed using an atomic force (AFM) microscope. The size, homogeneity and spherical morphology of the oil nanodroplets were confirmed by the AFM data and images, which revealed uniformly sized spherical particles with sizes from 110 to 150 nm for all nanoemulsions (Figure 2), as measured by the dynamic light scattering (DLS) in Zetasizer (Table 1).

Insert Table 1

Insert Figure 1

Insert Figure 2

With regard to their polydispersity, only nanoemulsions with encapsulated active compounds had PDI values lower than 0.20 over the 90-days storage (Table 1), displaying a monodisperse droplet size distribution (Figure 1) and showing a visual and physical stability, perhaps as a result of the optimal pressure and number of processing cycles used throughout the homogenization process, as reported in previous works by Tan & Nakajima (2005); Troncoso, Aguilera, & McClements (2012), and Pérez-Córdoba & Sobral, (2017). Although the PDI value for the control nanoemulsions was 0.20 upon formation, this shifted slightly to higher values as a small shoulder at size ranges of approximately 8µm developed during storage (Figure 1a). These results suggested that the microfluidizer was able to produce nanoemulsions from coarse emulsions containing polydisperse micrometers droplets (Supplementary Figure S1). Nanoemulsions with ζ-potential values greater than +30 mV or lower than -30 mV are expected to be highly stable since droplets are sufficiently charged to enable inter-particle repulsive forces to dominate (Heurtault, Saulnier, Pech, Proust, & Benoit, 2003; Salvia-Trujillo, Rojas-Graü, Soliva-Fortuny, & Martín-Belloso, 2013). As can be observed in Table 1, the negative ζ-potential values for all nanoemulsions were above this -30 mV threshold, potentially as a result of the adsorption of hydroxyl ions at the oil-water interface and subsequent development of hydrogen bonds between these ions and the ethylene oxide groups of the surfactant (Dias et al., 2014; Jo & Kwon, 2014). Nevertheless, despite their moderate magnitude, the resulting net charge differences in the tested nanoemulsions were able to contribute to the systems' high stability against creaming and/or flocculation phenomena during storage (Jo & Kwon, 2014).

In terms of pH, the control nanoemulsions were able to maintain a value of pH 6 for the duration of storage, whilst a significant ($p<0.05$) pH reduction was observed for all nanoemulsions with encapsulated active compounds. This behavior could be attributed to the production of acidic compounds (carboxylic acids) after the decomposition of hydroperoxides from the oxidation of the encapsulated lipophilic compounds (Cheong, Tan, & Nyam, 2017; Grill, Ogle, & Miller, 2006). Cheong et al., (2017) also observed the same pH reduction behavior and very close pH values for kenaf seed (*Hibiscus cannabinus* L.) oil-in-water nanoemulsion stored at 4 ºC. Hsu & Nacu (2003) affirm that an ideal pH value for O/W emulsions should be greater than 4.0 to ensure stability. Similarly,

Nejadmansouri et al. (2016) reported that, at higher pH values (pH>4), nanoemulsions remain relatively stable against droplet aggregation as a result of sufficient electrostatic repulsions between negatively charged droplets (Nejadmansouri et al., 2016).

3.1.3 Flow behavior of nanoemulsions

In this study, the viscosity was not dependent on the shear rate used for the sample test when measured at ambient temperature (20°C ±2°C). All prepared nanoemulsions presented viscosity values of approximately 10^{-3} mPa.s, being closer to the viscosity of water, and showed Newtonian behavior. This behavior could be attributed to that those nanoemulsions were prepared with an oil phase of 10% w/w. According to Floury, Desrumaux, Axelos, & Legrand, (2003), emulsions containing less than 20% (w/w) of the dispersed phase always show a Newtonian behavior, regardless of the homogenization pressure or another condition applied in their preparation. Alexandre et al. (2016) obtained similar flow behavior when preparing O/W nanoemulsion loaded with ginger essential oil. This rheological behavior can be considered as interesting because water is the solvent usually used in the biopolymer-based film preparation (Alexandre et al. 2016).

3.2 Film characterization

Films prepared without (N_0) or with nanoemulsions (N_1, N_2, N_3, or N_4) were visually homogeneous with no cracks, scratches, bubbles, or visible phase separation. Film thickness was well maintained by controlling the mass ratio of FFS/dish area and thus remained constant at 0.080 ± 0.002 mm ($p>0.05$) across all film formulations (Table 2). According to Benbettaïeb et al. (2014), controlling thickness is key for ensuring the films' physical and barrier properties.

Insert Table 2

3.2.1 Moisture content, solubility in water and swelling

No significant difference ($p>0.05$) was observed in the moisture content (MC) of all samples (Table 2), which was maintained at approximately 18%. It is therefore evident that the oil phase fraction in the nanoemulsions was relatively low and did not affect the hygroscopicity of the produced films, which was predominantly dictated by the biopolymer matrix (Pérez-Córdoba & Sobral, 2017).

Solubility is another important film characteristic that can affect film integrity as well as the migration of the encapsulated bioactive compounds into the foodstuff (Mihaly Cozmuta et al., 2015). All films loaded with nanoemulsions (N_1, N_2, N_3, or N_4) presented slightly lower ($p<0.05$) solubility in water (SW) than the control 1 film (N_0); SW values for the former were between 43.1 and 48.9%, with films loaded with N_2 and N_3 exhibiting the lowest SW ($p>0.05$) (Table 2).

Ahmad et al. (2012) reported a reduction on the water solubility of gelatin-based films following the incorporation of bergamot and lemongrass oil. This was presumably due to the non-polar

components in the used oils, which resulted in a substantial physical interference in the entanglement of gelatin polypeptide chains within the film matrix. Such interference, which might have led to a significant blockade on the capacity of gelatin to interact with water molecules, would be mainly responsible for reducing the water solubility of the composite films (Hosseini et al., 2013; Mihaly Cozmuta et al., 2015).

These SW values were similar to those reported by Ma et al. (2012) (44.7 %) and Gómez-Estaca, López de Lacey, López-Caballero, Gómez-Guillén, & Montero (2010) (41.1%) for gelatin or gelatin-chitosan based films loaded with nanoemulsified olive or clove oil droplets in water, respectively. This was attributed to the establishment of protein-polyphenol interactions which weaken the interactions that stabilize the protein network (Gómez-Estaca et al., 2010). On the other hand, Jridi et al. (2014) reported higher SW (85.6%), and Benbettaïeb et al. (2014), Hosseini et al. (2013), and Gómez-Estaca et al. (2010) obtained lower SW values for G-Ch (37.8 – 39.1%) or G-Ch films loaded with essential clove oil (29.5%) than those obtained in this work. This evidence demonstrates that SW does not correspond to a simple rule of mixing and may result from interactions between both gelatin and chitosan caused by electrostatic forces, hydrogen bonding, etc, or by the presence of droplets oil that stabilize the film structure (Jridi et al., 2014; Pereda et al., 2011), as will be discussed in section 3.2.4 and seen in the X-ray diffractograms (Figure 3).

Despite its highest SW, the control 1 film (N_0) displayed the lowest ability to swell (26.9 g/g) as well as the greatest ($p<0.05$) surface hydrophobicity amongst all tested samples; the latter was evaluated by contact angle measurements (data not shown). Although film swelling (S) was found to vary between different systems ($p<0.05$), this was not dependent on the incorporation (or not) of the nanoemulsion, with the N_1 and N_4 films, displaying the highest (30 g/g) and lowest (25.3 g/g) swelling, respectively. Nonetheless it is expected that these films would exhibit a high degree of swelling due to the great water uptake capacity of gelatin and also the porous structure of its polymeric network (Kavoosi, Mohammad, Dadfar, Purfard, & Mehrabi, 2013).

3.2.2 Mechanical properties

The N_0 films displayed the highest ($p < 0.05$) tensile strength (TS) and the lowest elongation at break (EB) values among all samples (Table 2); 19.0 MPa and 89.1%, respectively. In comparison to N_0 films, films loaded with nanoemulsions showed a considerable reduction in TS, as well as an increase in their EB values, a typical behavior of plasticized films (Sobral et al., 2001). This is in agreement with previous studies reporting that addition of lipophilic species (e.g. essential oils or fatty acids) decreases the TS values of biopolymer-based films; e.g., films from gelatin (Limpisophon, Tanaka, & Osako, 2010; Tongnuanchan, Benjakul, & Prodpran, 2013), chitosan (Martins, Cerqueira, & Vicente, 2012; Rubilar et al., 2013) or whey protein (Soazo, Rubiolo, & Verdini, 2011), etc. This has been attributed to the inability of lipids to form continuous and cohesive matrices (Péroval, Debeaufort, Despré, & Voilley, 2002; Rubilar et al., 2013).

EB results obtained here are comparable to those reported by Kavoosi et al. (2013) and Tongnuanchan, Benjakul, & Prodpran (2014) for gelatin based films; who obtained EB mean values of 128% and 114%, respectively, and, similarly to the present study, a significant ($p<0.05$) decrease in TS when carvacrol, and basil or lemon essential oils were incorporated into the gelatin films. Similarly, Hosseini, Rezaei, Zandi, & Farahmandghavi (2016) reported a significant ($p<0.05$) increase in EB value (reaching a maximum value of 151.8%) for gelatin/chitosan based films emulsified with oregano oil (0.4% w/v) and also a reduction of 69% in its original tensile strength. This behavior has been attributed to the chemical nature of the films' biopolymeric components and the plasticizing role of the essential oil (loaded onto the matrix), resulting in the enhancement of their ductile properties (Hosseini et al., 2016; Tongnuanchan et al., 2012).

With regard to the EM results, the addition of nanoemulsions into the polymeric-blend matrix leads to a significant ($p<0.05$) reduction of the films' stiffness. The highest (71.4%) and lowest (61.3%) EM reduction was observed for N_1 and N_4 films, respectively (Table 2). Hosseini et al. (2016) also reported a significant ($p<0.05$) decrease on EM when different oregano oil concentrations were added into gelatin-chitosan based films. Similarly, Tongnuanchan et al. (2014) reported a significant ($p<0.05$) reduction of EM for gelatin based films loaded with different essential oils (basil, plai and lemon), in respect to the control film (without essential oils).

3.2.3 Light transmission and opacity

Incorporation of the N_1 nanoemulsion within the gelatin-chitosan film (control 2) significantly reduces the transmittance values in the wavelength range of 250 - 280 nm (Table 3) in comparison to those of N_0 films (control 1). These transmittance values are then further reduced by the incorporation of α-t, Cin, and/or GO within the nanodroplets, thus indicating that the formulated films act as excellent barriers to radiation in the ultraviolet (UV) light region when compared with both control films (N_0 and N_1). In addition to the aromatic rings of amino acid residues from the gelatin molecule, this protective capacity of the films is envisaged to be enhanced by the chemical structure of the encapsulated compounds which contain phenolic groups (Bonilla & Sobral, 2016; Dammak, Carvalho, Trindade, Lourenço, & Sobral, 2017). Good UV and visible light barrier properties in the 200 - 350 nm range were also found by Gómez-Estaca, Giménez, Montero, & Gómez-Guillén (2009) and Wu et al. (2013) in gelatin-based films containing oregano or green tea extracts, respectively. In the visible range (350 - 800 nm), the N_0 films showed the highest ($p<0.05$) light transmission (80-97%) when compared to films loaded with N_1, N_2, N_3, or N_4 (Table 3). These values were similar to those reported by Jridi et al. (2014) for gelatin-chitosan composite films (72.6-90.9%) and higher than those reported by Dammak et al. (2017) for pure gelatin-based films (45–56%). Hence, it can be seen that chitosan has a significant contribution in terms of light transmission in the visible range (Jridi et al., 2014).

Insert Table 3

On the other hand, the transparency of films differed significantly ($p<0.05$) among samples, when nanoemulsions were added, as evidenced in Table 3. This transparency values are directly associated with the film opacity (i.e, the N_1 films presented the highest transparency value and the greatest opacity). In this case, the N_0 films was the most transparent, however when adding the different nanoemulsions became opaque, maybe due to the nanoencapsulated active compounds (NAC), which were able to impede the light transmission through the films (Tongnuanchan et al., 2012) or due to the formation of poly-anion/cation complexes between the gelatin-chitosan matrix and the nanoemulsions (Jridi et al., 2014). Tongnuanchan et al. (2012) also reported that emulsified essential oil droplets incorporated into a gelatin based film lowered its transparency, likely due to the light scattering effect. The transparency values of the films loaded with N_1, N_2, N_3, and N_4 were quite close to those opacity values previously reported by Rivero et al. (2009) for composite and bi-layer films based on gelatin and chitosan (0.68 – 0.99), while the N_0 films showed a transparency value lower than that reported by Jridi et al. (2014) for gelatin-chitosan based films (0.99 ± 0.12).

3.2.4 X-ray diffraction

The presence of a strong interaction between the biopolymer matrix and NAC was confirmed by X-ray diffraction (XRD) analysis. All films exhibited an X-ray diffraction pattern characteristic of a partially crystalline material (Figure 3), with two defined diffraction peaks, the first in the region of $2\theta = 10^{o}$, corresponding either to the crystalline triple helix structure of gelatin or the relatively regular crystal lattice of chitosan, and a second broader band at $2\theta = 20^{o}$, characteristic of an amorphous phase (Pereda et al., 2011; Valencia, Lourenço, Bittante, & Sobral, 2016). Peaks observed in the films at approximately 32^{o} could be assigned to the (020) diffraction plane of hydrated chitosan crystals and relate to the films' preparation procedure (i.e. dissolution of chitosan in an acetic acid solution) or the chemical structure of the active compound incorporated (Pereda et al., 2011).

The incorporated active compounds through nanoemulsions N_2, N_3 and N_4, slightly changed the highest peak intensity, but in general, the profile of diffraction spectra of these films was similar to those obtained for the control films (N_0 and N_1). The increase in the intensity of the peaks at 10^{o} for the N_3 and N_4 films, indicates that incorporation of nanoencapsulated GO into the biopolymer-blend matrix induces an increase in the films' crystallinity. A similar effect was observed by Rubilar et al. (2013) when incorporating carvacrol into chitosan based films. In contrast, Valenzuela, Abugoch, & Tapia (2013) reported that the introduction of sunflower oil into a quinoa protein–chitosan based film generated a structure less crystalline, whilst Alexandre et al. (2016) reported no effect on the crystallinity of gelatin based films when a ginger essential oil-loaded nanoemulsion was incorporated.

Insert Figure 3

3.2.5 Thermal properties

In general, all films exhibited similar differential scanning calorimetry (DSC) curves (Figure 4). Curves from the first scan revealed a trace typical for partially crystalline material, with a glass transition, attributed to a fraction rich in gelatin, followed by a marked endothermal peak, associated to a helix-coil transition (Sobral et al., 2001; Valencia et al., 2016). In the second scan, a typical trace for amorphous material was observed, where a glass transition also occurred (Alexandre et al., 2016).

Insert Figure 4

The glass transition temperatures (T_g) of all films did not appear to be affected by formulation characteristics ($p>0.05$), remaining at approximately 46ºC and 10ºC, in the first and second scan, respectively (Table 4). T_g values were in agreement to those reported by Gómez-Estaca et al. (2009) for films based on gelatin incorporated with extracts (T_g = 42 - 47ºC) and by Hosseini et al. (2013) for a blend of gelatin-chitosan with no incorporated species (T_g = 45 - 56ºC).

All films showed a crystal melting temperature (T_m) at approximately 55ºC ($p>0.05$). Nevertheless, only films loaded with the nanoemulsions exhibited an additional marked endothermal peak at -18ºC in both scans (Figure 5), which can be either attributed to the T_m of the canola oil (-10 ºC) used for encapsulating the active compounds in nanodroplets, or even to the T_m of the NAC themselves. Ma et al. (2012) also reported an extra endothermal peak at -8ºC, attributed to the melting of olive oil that was emulsified into gelatin based films.

With regard to melting enthalpy (ΔH_g), this was significantly ($p<0.05$) reduced from 12.1 J/g (N_0 films) to approximately 9.0 J/g when the films were loaded with N_1, N_2, N_3, or N_4 (Table 4). The higher enthalpy value for the N_0 films indicated that they had a higher level of renaturation compared to the nanoemulsion-loaded films, leading to an improved strength value (Jridi et al., 2014), as demonstrated by the TS data (Table 2). It is possible that the inter-chain distances of the gelatin macromolecules increased with nanoemulsions-loaded films and this is expected to decrease the entanglement of the gelatin chains and to increase their molecular mobility, reducing the melting enthalpy. Alexandre et al. (2016) also observed a reduction in the ΔH_g for films gelatin based films when ginger oil loaded-nanoemulsions were incorporated into the film matrix. However, Jridi et al. (2014) reported higher T_g (64.7ºC) and ΔH_g (66.4 J/g) values and no T_m for fish skin gelatin-chitosan based films, maybe due to a better level of blending after intermolecular interaction between the gelatin and chitosan (Jridi et al., 2014). .

3.2.6 Atomic force microscopy

Atomic force microscopy (AFM) analyses were performed to observe the effect of nanoemulsions incorporation on the surface topography of the films. Typical 3-D and 2-D surface topographic AFM images are presented in Figure 5. The incorporation of the nanoemulsions into the biopolymeric matrix led to a marked increase in both the average (R_a) and root-mean-square (R_q) roughness of the films (Table 4). The R_q increased drastically from 11.1 nm (N_0 films) to a maximum value of 58.6 nm (N_1 films) following the loading N_1, N_2, N_3, or N_4 into the films. The R_a values showed a similar trend, increasing from 7.45 nm to 44.14 nm. Atarés, Bonilla, & Chiralt (2010), Hosseini et al. (2016), and Ma et al. (2012) have also reported an increase in terms of film roughness as a result of the incorporation of ginger oil, oregano oil, or olive oil into sodium caseinate, gelatin-chitosan blend, or gelatin based films, respectively. It has been proposed that this trend is potentially due to an enhancement in lipid aggregation and/or creaming phenomena, which are exacerbated by the drying step and ultimately result in an elevated level of irregularities on the films' surfaces (Ma et al., 2012).

Insert Figure 5

Insert Table 4

3.2.7 Environmental scanning electron microscopy (ESEM)

The environmental scanning electron microscopy (ESEM) micrographs of the surface and cross-sectional morphology of the films revealed a continuous and homogeneous microstructure, without the presence of scratches, phase separation, and/or porosity due to the presence of trapped air cells (Figure 6). Furthermore, no evidence of oil droplets separation from the biopolymer-blend matrix was observed in the films loaded with nanoemulsions. However, the previously determined roughness difference between the N_0 film and the ones loaded with N_1, N_2, N_3, or N_4 (Table 4) was also confirmed by the ESEM analysis (Figure 6). The marked roughness that was visible in the cross-sectional images of the films loaded with nanoemulsions has been previously reported by Hoque, Benjakul, & Prodpran (2011), Hosseini et al. (2016), and Pérez-Córdoba & Sobral (2017) for gelatin films or blends when these were loaded with some extract or essential oils (i.e. cinnamon, clove or star anise extracts and oregano or garlic oil).

Amongst the samples loaded with nanoemulsions, the N_1 films appeared to possess the highest degree of surface and cross-sectional roughness, in agreement with the roughness data from AFM analyses (Figure 5). Then, this also suggests that NAC enhance the film roughness when incorporated into the matrix. Similarly, Acevedo-Fani et al. (2015), Chen et al. (2016), and Pérez-Córdoba & Sobral (2017) have reported an improvement in the microstructures of films based on biopolymer blends when mixed with nanoemulsified essential oils.

Insert Figure 6

3.2.8 Antimicrobial Activity

The inhibitory activity against both *P. aeruginosa* (Gram negative) and *L. monocytogenes* (Gram positive) was determined measuring the clear zone surrounding the disks (inhibition zone). Halo formation (65 - 138 mm^2) around the active films was observed only in the case of *P. aeruginosa*, which exhibited greater sensitivity compared to *L. monocytogenes* (Table 5). Similar observations were reported by Hafsa et al. (2016) and Kavoosi et al. (2014) when tested chitosan and gelatin based films with incorporated Eucalyptus globulus or Zataria multiflora essential oils. Paparella et al. (2008) suggested that the antimicrobial activity of some essential oils, is due to their interaction with enzymes located on the cell wall or the breakdown of the phospholipids present in the cell membrane, which results to increased permeability and leakage of cytoplasm.

The antimicrobial effect against *P. aeruginosa* could have been enhanced by the presence of chitosan in the blend, which has been widely reported as an antimicrobial compound (Elsabee & Abdou, 2013; Pranoto et al., 2005; Yuan, Chen, & Li, 2016). This has been ascribed to the presence of positively charged amino groups in the chitosan structure, which interact with the negatively charged microbial cell membranes and lead to the leakage of proteinaceous (and other intracellular) constituents from the microorganisms (Pereda et al., 2011, Pranoto et al., 2005). However, in this study all the G-Ch based films without active compounds (N_0 and N_1) showed no activity against the tested bacteria (Table 5).

When active films were tested against *L. monocytogenes*, inhibition zones were not obvious ($p>0.05$); however, a clear zone was observed underneath the films. This observation could be associated to the limited diffusion of NAC from the films to the media (Pereda et al., 2011; Ponce, Roura, del Valle, & Moreira, 2008) since in our case the active compounds were doubly encapsulated, into the nanodroplets and in the film matrix. Otoni et al. (2014), Seydim & Sarikus (2006) and Sung et al. (2014) have reported activity against *L. monocytogenes* when using nanoemulsified cinnamaldehyde or GO into pectin/papaya puree, whey protein and low-density-polyethylene/ethylene-vinyl-acetate based films. In our study, nanoemulsified active compounds when not tested in films, showed high activity against *L. monocytogenes* (data not shown), which could be considered a derivative of the antimicrobial compounds and their delivery through nano-sized droplets, as reported by Kadri et al. (2017).

Converse to expectation, the combined application of nanoencapsulated Cin and GO within the film did not enhance the antimicrobial properties of the G-Ch based film ($p<0.05$), although both of them had the ability to induce an inhibitory effect as bulk agent on the microorganism tested, principally due to their chemical components, such as cinnamic aldehyde and diallyl trisulfide, diallyl disulphide, methyl allyl trisulfide, and diallyl tetrasulfide, which are able to disrupt and penetrate the lipid structure of the bacteria cell membrane, leading to its destruction (Peng & Li, 2014).

3.2.9 Antioxidant properties

The antioxidant activity of the films expressed as trolox equivalent (μmol TE /g dried film) for the $DPPH^{\bullet}$ and $ABTS^{\bullet+}$ radicals, and the FRAP reagent is shown in Table 5. As expected, the control 1 film did not show any radical scavenging activity, in either of the $DPPH^{\bullet}$ or $ABTS^{\bullet+}$ tested method, and possessed very low FRAP scavenging activity.

Films loaded with NAC were capable of acting as stronger donors of hydrogen atoms or electrons until reduction of the stable purple-coloured radical $DPPH^{\bullet}$ or blue-coloured radical $ABTS^{\bullet+}$ converted to yellow-coloured DPPH-H or $ABTS^{\bullet}$, respectively (Brand-Williams et al., 1995; Re et al., 1999). The film loaded with the nanoemulsion encapsulating α-t/Cin (N_2) exhibited the greatest antioxidant activity for both $DPPH^{\bullet}$ and $ABTS^{\bullet+}$ radicals, with values of 0.22 ± 0.02 and 2.63 ± 0.12 μmol TE/g film, respectively. This activity corresponded to the highest radical scavenging effect of that nanoemulsion (N_2) before incorporating in the film (data not shown). The results for $ABTS^{\bullet+}$ radical scavenging of the films were comparable to those reported by Bonilla & Sobral (2016) and Pérez-Córdoba & Sobral (2017) for gelatin-chitosan based films loaded with boldo or guarana extracts, and nanoemulsified active compounds, respectively.

On the other hand, the incorporation of α-t/GO-loaded nanoemulsion (N_3) into the film caused the highest ($p<0.05$) ferric reducing ability and, consequently, the best antioxidant activity measured by the FRAP assay with an increase of 91% and 51%, respectively, when compared with either of the two control films (N_0 and N_1). The FRAP assay gave the highest TE values, probably because of the direct contact of the film samples with the FRAP reagent during the reaction.

The antioxidant activity of the films is potentially attributed to the phenolic acids and terpenoids coming from the cinnamaldehyde, garlic oil, and principally, α-tocopherol, which are able to quench free radicals by forming resonance-stabilized phenoxyl radicals (Dudonné, Vitrac, Coutière, Woillez, & Mérillon, 2009). In addition to this, the contribution from the residual free amino groups of the chitosan molecule, which also react with free radicals forming stable macromolecular radicals and ammonium groups, should also be taken into account in terms of antioxidant activity (Yen, Yan, & Mau, 2008; Yuan et al., 2016).

Insert Table 5

4. Conclusions

O/W emulsions, with α-toc, Cin and GO active compounds loaded within their dispersed phase droplets at high encapsulation efficiencies, were successfully formed at the nanoscale via a microfluidization technique. The formed nanoemulsions possessed a monomodal distribution and exhibited good physical stability over a 90 days storage and incorporation of the active species was not detrimental to either of these features. These nanoemulsions were subsequently incorporated into gelatin-chitosan (G-Ch) based films, which were shown to possess a homogeneous structure with a

good distribution of nanoencapsulated active compounds (NAC) throughout the biopolymer matrix and without any unfavorable effects ($p>0.05$) on the films' original thickness, moisture content, glass transition, and melting temperature.

Nanoemulsion loading was found to enhance the films' resistance to water, reducing ($p<0.05$) their solubility, and increasing film elongation at break and light barrier properties, while also directly affecting their transparency, reducing their tensile strength and stiffness, and increasing their surface roughness. Therefore, nanoemulsions encapsulating active compounds are suitable to produce G-Ch based films, enhancing their physical and mechanical properties, antibacterial performance against *L. monocytogenes* and *P. aeruginosa*, and their radicals scavenging effect.

Films loaded with NAC have a potential applications in food packaging for food shelf-life improvement.Further studies on controlled release and foodstuff application are needed to know the real advantage of those active films when used on food.

Acknowledgements: To São Paulo Research Foundation (FAPESP) for first author's PhD fellowships (13/14324-2 and 15/22285-2). Work of the CEPID-FoRC (13/07914-8). Authors also thank the support of Paolo Passareti in AFM analyses, a PhD student at the University of Birmingham, and Michael Stablein for English revision, a Master student at the University of Illinois.

Conflict of interest

Authors declare that this work has not been published previously and there are no conflicts of interest.

References

Abdollahi, M., Rezaei, M., & Farzi, G. (2012). A novel active bionanocomposite film incorporating rosemary essential oil and nanoclay into chitosan. *Journal of Food Engineering*, *111*(2), 343 - 350. https://doi.org/10.1016/j.jfoodeng.2012.02.012

Acevedo-Fani, A., Salvia-Trujillo, L., Rojas-Graü, M. A., & Martín-Belloso, O. (2015). Edible films from essential-oil-loaded nanoemulsions: Physicochemical characterization and antimicrobial properties. *Food Hydrocolloids*, *47*, 168–177. https://doi.org/10.1016/j.foodhyd.2015.01.032

Ahmad, M., Benjakul, S., Prodpran, T., & Agustini, T. W. (2012). Physico-mechanical and antimicrobial properties of gelatin film from the skin of unicorn leatherjacket incorporated with essential oils. *Food Hydrocolloids*, *28*(1), 189–199. https://doi.org/10.1016/j.foodhyd.2011.12.003

Alexandre, E. M. C., Lourenço, R. V., Quinta Barbosa Bittante, A. M., Moraes, I. C. F., & Sobral, P. J. do A. (2016). Gelatin-based films reinforced with montmorillonite and activated with nanoemulsion of ginger essential oil for food packaging applications. *Food Packaging and Shelf Life*, *10*, 87–96.

American Society for Testing and Materials D882/12 (2001). Standard Test Method for tensile properties of thin plastic sheeting. In Annual book of ASTM standards. http://dx.doi.org/10.1520/D0882-12

Anarjan, N., Mirhosseini, H., Baharin, B. S., & Tan, C. P. (2011). Effect of processing conditions on physicochemical properties of sodium caseinate-stabilized astaxanthin nanodispersions. *LWT - Food Science and Technology*, *44*(7), 1658–1665. https://doi.org/10.1016/j.lwt.2011.01.013

Arancibia, M., Giménez, B., López-Caballero, M. E., Gómez-Guillén, M. C., & Montero, P. (2014). Release of cinnamon essential oil from polysaccharide bilayer films and its use for microbial growth inhibition in chilled shrimps. *LWT - Food Science and Technology*, *59*, 989–995. https://doi.org/10.1016/j.lwt.2014.06.031

Atarés, L., Bonilla, J., & Chiralt, A. (2010). Characterization of sodium caseinate-based edible films incorporated with cinnamon or ginger essential oils. *Journal of Food Engineering*, *100*(4), 678 - 687. https://doi.org/10.1016/j.jfoodeng.2010.05.018

Baron, R. D., Pérez, L. L., Salcedo, J. M., Córdoba, L. P., & Sobral, P. J. do A. (2017). Production and characterization of films based on blends of chitosan from blue crab (Callinectes sapidus) waste and pectin from Orange (Citrus sinensis Osbeck) peel. *International Journal of Biological Macromolecules*, *98*, 676–683. https://doi.org/10.1016/j.ijbiomac.2017.02.004

739 Benbettaïeb, N., Kurek, M., Bornaz, S., & Debeaufort, F. (2014). Barrier, structural and mechanical properties of bovine
740 gelatin-chitosan blend films related to biopolymer interactions. *Journal of the Science of Food and Agriculture*,
741 *94*(12), 2409–2419. https://doi.org/10.1002/jsfa.6570
742 Bonilla, J., & Sobral, P. J. A. (2016). Investigation of the physicochemical, antimicrobial and antioxidant properties of
743 gelatin-chitosan edible film mixed with plant ethanolic extracts. *Food Bioscience*, *16*, 17–25.
744 https://doi.org/10.1016/j.fbio.2016.07.003
745 Brand-Williams, W., Cuvelier, M. E., & Berset, C. (1995). Use of a free radical method to evaluate antioxidant activity.
746 *LWT - Food Science and Technology*, *28*(1), 25–30. https://doi.org/10.1016/S0023-6438(95)80008-5
747 Chen, H., Hu, X., Chen, E., Wu, S., Mcclements, D. J., Liu, S., & Li, Y. (2016). Preparation, characterization, and properties
748 of chitosan films with cinnamaldehyde nanoemulsions. *Food Hydrocolloids*, *61*, 662–671.
749 https://doi.org/10.1016/j.foodhyd.2016.06.034
750 Cheong, A. M., Tan, C. P., & Nyam, K. L. (2017). Oil-in-water nanoemulsions under different storage temperatures.
751 *Industrial Crops and Products*, *95*, 374–382.
752 Cheong, J. N., Tan, C. P., Man, Y. B. C., & Misran, M. (2008). α-Tocopherol nanodispersions: Preparation, characterization
753 and stability evaluation. *Journal of Food Engineering*, *89*(2), 204–209. https://doi.org/10.1016/j.jfoodeng.2008.04.018
754 Dammak, I., Carvalho, R. A. de C., Trindade, C. S. F., Lourenço, R., & Sobral, P. J. A. (2017). Properties of active gelatin
755 films loaded with rutin-loaded nanoemulsions. *International Journal of Biological Macromolecules*, *98*, 39–49.
756 https://doi.org/http://dx.doi.org/10.1016/j.ijbiomac.2017.01.094
757 Dammak, I., & Sobral, P. J. A. (2017). Formulation and Stability Characterization of Rutin-Loaded Oil-in-Water Emulsions.
758 *Food and Bioprocess Technology*, *10*(5), 926–939. https://doi.org/10.1007/s11947-017-1876-5
759 Davidov-Pardo, G., & McClements, D. J. (2015). Nutraceutical delivery systems : Resveratrol encapsulation in grape seed
760 oil nanoemulsions formed by spontaneous emulsification. *Food Chemistry*, *167*, 205–212.
761 https://doi.org/10.1016/j.foodchem.2014.06.082
762 Dias, D. D. O., Colombo, M., Kelmann, R. G., Kaiser, S., Lucca, L. G., Teixeira, H. F., & Koester, L. S. (2014).
763 Optimization of Copaiba oil-based nanoemulsions obtained by different preparation methods. *Industrial Crops &*
764 *Products*, *59*, 154–162. https://doi.org/10.1016/j.indcrop.2014.05.007
765 Donsì, F., Annunziata, M., Sessa, M., & Ferrari, G. (2011). Nanoencapsulation of essential oils to enhance their
766 antimicrobial activity in foods. *LWT - Food Science and Technology*, *44*(9), 1908–1914.
767 https://doi.org/10.1016/j.lwt.2011.03.003
768 Donsì, F., Annunziata, M., Vincensi, M., & Ferrari, G. (2012). Design of nanoemulsion-based delivery systems of natural
769 antimicrobials : Effect of the emulsifier. *Journal of Biotechnology*, *159*(4), 342–350.
770 https://doi.org/10.1016/j.jbiotec.2011.07.001
771 Dudonné, S., Vitrac, X., Coutière, P., Woillez, M., & Mérillon, J.-M. (2009). Comparative Study of Antioxidant Properties
772 and Total Phenolic Content of 30 Plant Extracts of Industrial Interest Using DPPH, ABTS, FRAP, SOD, and ORAC
773 Assays. *Journal of Agricultural and Food Chemistry*, *57*(5), 1768–1774. https://doi.org/10.1021/jf803011r
774 Elsabee, M. Z., & Abdou, E. S. (2013). Chitosan based edible films and coatings: a review. *Materials Science &*
775 *Engineering. C, Materials for Biological Applications*, *33*(4), 1819–41. https://doi.org/10.1016/j.msec.2013.01.010
776 Fathi, M., Mozafari, M. R., & Mohebbi, M. (2012). Nanoencapsulation of food ingredients using lipid based delivery
777 systems. *Trends in Food Science and Technology*, *23*(1), 13–27. https://doi.org/10.1016/j.tifs.2011.08.003
778 Ferreira, A. S., Nunes, C., Castro, A., Ferreira, P., & Coimbra, M. A. (2014). Influence of grape pomace extract
779 incorporation on chitosan films properties. *Carbohydrate Polymers*, *113*, 490–499.
780 https://doi.org/10.1016/j.carbpol.2014.07.032
781 Floury, J., Desrumaux, A., Axelos, M. a V, & Legrand, J. (2003). Effect of high pressure homogenisation on methylcellulose
782 as food emulsifier. *Journal of Food Engineering*, *58*(3), 227–238. https://doi.org/10.1016/S0260-8774(02)00372-2
783 Gennadios, A., McHugh, T. H., Weller, C. L., & Krochta, J. M. (1994). Edible coatings and films based on proteins. In:
784 *Edible Coat. Films Improve Food Qual.* (Krochta, J. M., Baldwin, E. A., and Nisperos-Carriedo, M. O., eds.), pp.
785 201–277. Technomic Publishing Company, Inc., Lancaster, PA.
786 Gómez-Estaca, J., Giménez, B., Montero, P., & Gómez-Guillén, M. C. (2009). Incorporation of antioxidant borage extract
787 into edible films based on sole skin gelatin or a commercial fish gelatin. *Journal of Food Engineering*, *92*(1), 78–85.
788 https://doi.org/10.1016/j.jfoodeng.2008.10.024
789 Gómez-Estaca, J., López de Lacey, A., López-Caballero, M. E., Gómez-Guillén, M. C., & Montero, P. (2010).
790 Biodegradable gelatin-chitosan films incorporated with essential oils as antimicrobial agents for fish preservation.
791 *Food Microbiology*, *27*(7), 889–96. https://doi.org/10.1016/j.fm.2010.05.012
792 Gómez-Guillén, M. C., Pérez-Mateos, M., Gómez-Estaca, J., López-Caballero, E., Giménez, B., & Montero, P. (2009). Fish
793 gelatin: a renewable material for developing active biodegradable films. *Trends in Food Science and Technology*,
794 *20*(1), 3 - 16. https://doi.org/10.1016/j.tifs.2008.10.002
795 Gontard, N. ; Duchez, C.; Cuq, J.L. ; Guilbert, S. (1994). Edible composite films of wheat gluten and lipids: water vapour
796 permeability and others physical properties. *International Journal of Food Science and Technology*, *29*, 39–50.
797 https://doi.org/10.1111/j.1365-2621.1994.tb02045.
798 Grill, J. M., Ogle, J, & Miller, S. A. (2006). An Efficient and Practical System for the Catalytic Oxidation of Alcohols,
799 Aldehydes, and α,β-Unsaturated Carboxylic Acids. *The Journal of Organic Chemistry*, *71*(25), 9291 - 9296.
800 https://doi.org/10.1021/JO0612574
801 Hafsa, J., Smach, M. ali, Ben Khedher, M. R., Charfeddine, B., Limem, K., Majdoub, H., & Rouatbi, S. (2016). Physical,
802 antioxidant and antimicrobial properties of chitosan films containing Eucalyptus globulus essential oil. *LWT - Food*
803 *Science and Technology*, *68*, 356–364. https://doi.org/10.1016/j.lwt.2015.12.050
804 Heurtault, B., Saulnier, P., Pech, B., Proust, J. E., & Benoit, J. P. (2003). Physico-chemical stability of colloidal lipid
805 particles. *Biomaterials*, *24*(23), 4283–4300. https://doi.org/10.1016/S0142-9612(03)00331-4

Hoque, M. S., Benjakul, S., & Prodpran, T. (2011). Properties of film from cuttlefish (Sepia pharaonis) skin gelatin incorporated with cinnamon, clove and star anise extracts. *Food Hydrocolloids*, *25*(5), 1085–1097. https://doi.org/10.1016/j.foodhyd.2010.10.005

Hosseini, S., Rezaei, M., Zandi, M., & Ghavi, F. F. (2013). Preparation and functional properties of fish gelatin-chitosan blend edible films. *Food Chemistry*, *136*(3–4) 1490 - 1495. https://doi.org/10.1016/j.foodchem.2012.09.081

Hosseini, S. F., Rezaei, M., Zandi, M., & Farahmandghavi, F. (2016). Development of bioactive fish gelatin/chitosan nanoparticles composite films with antimicrobial properties. *Food Chemistry*, *194*, 1266–1274. https://doi.org/10.1016/j.foodchem.2015.09.004

Hsu, J. P., & Nacu, A. (2003). Behavior of soybean oil-in-water emulsion stabilized by nonionic surfactant. *Journal of Colloid and Interface Science*, *259*(2), 374–381. https://doi.org/10.1016/S0021-9797(02)00207-2

Jo, Y. J., & Kwon, Y. J. (2014). Characterization of β-carotene nanoemulsions prepared by microfluidization technique. *Food Science and Biotechnology*, *23*(1), 107–113. https://doi.org/10.1007/s10068-014-0014-7

Jridi, M., Hajji, S., Ayed, H. Ben, Lassoued, I., Mbarek, A., Kammoun, M., & Nasri, M. (2014). Physical, structural, antioxidant and antimicrobial properties of gelatin-chitosan composite edible films. *International Journal of Biological Macromolecules*, *67*, 373 - 379. https://doi.org/10.1016/j.ijbiomac.2014.03.054

Kadri, H. El, Devanthi, P. V. P., Overton, T. W., & Gkatzionis, K. (2017). Do oil-in-water (O/W) nano-emulsions have an effect on survival and growth of bacteria? *Food Research International*, *101*, 114–128. https://doi.org/10.1016/j.foodres.2017.08.064

Kanatt, S. R., Rao, M. S., Chawla, S. P., & Sharma, A. (2012). Active chitosan–polyvinyl alcohol films with natural extracts. *Food Hydrocolloids*, *29* (2), 290–297. https://doi.org/10.1016/j.foodhyd.2012.03.005

Kavoosi, G., Mohammad, S., Dadfar, M., Purfard, A. M., & Mehrabi, R. (2013). Antioxidant and antibacterial properties of gelatin films incorporated with carvacrol. *Journal of Food Safety*, *33*(4), 423 - 432. https://doi.org/10.1111/jfs.12071

Kavoosi, G., Rahmatollahi, A., Mohammad Mahdi Dadfar, S., & Mohammadi Purfard, A. (2014). Effects of essential oil on the water binding capacity, physico-mechanical properties, antioxidant and antibacterial activity of gelatin films. *LWT - Food Science and Technology*, *57*, 556–561. https://doi.org/10.1016/j.lwt.2014.02.008

Kurek, M., Galus, S., & Debeaufort, F. (2014). Surface, mechanical and barrier properties of bio-based composite films based on chitosan and whey protein. *Food Packaging and Shelf Life*, *1*, 56–67. https://doi.org/10.1016/j.fpsl.2014.01.001

Limpisophon, K., Tanaka, M., & Osako, K. (2010). Characterisation of gelatin–fatty acid emulsion films based on blue shark (Prionace glauca) skin gelatin. *Food Chemistry*, *122*(4), 1095–1101. https://doi.org/10.1016/j.foodchem.2010.03.090

Ma, W., Tang, C.-H., Yin, S.-W., Yang, X.-Q., Wang, Q., Liu, F., & Wei, Z.-H. (2012). Characterization of gelatin-based edible films incorporated with olive oil. *Food Research International*, *49*(1), 572–579. https://doi.org/10.1016/j.foodres.2012.07.037

Mao, L., Yang, J., Xu, D., Yuan, F., & Gao, Y. (2010). Effects of Homogenization Models and Emulsifiers on the Physicochemical Properties of β-Carotene Nanoemulsions. *Journal of Dispersion Science and Technology*, *31*(7), 986–993. https://doi.org/10.1080/01932690903224482

Martins, J. T., Cerqueira, M. A., & Vicente, A. A. (2012). Influence of α-tocopherol on physicochemical properties of chitosan-based films. *Food Hydrocolloids*, *27*(1), 220–227. https://doi.org/10.1016/j.foodhyd.2011.06.011

Mihaly Cozmuta, A., Turila, A., Apjok, R., Ciocian, A., Mihaly Cozmuta, L., Peter, A., & Benković, T. (2015). Preparation and characterization of improved gelatin films incorporating hemp and sage oils. *Food Hydrocolloids*, *49*, 144–155. https://doi.org/10.1016/j.foodhyd.2015.03.022

Nejadmansouri, M., Mohammad, S., Hosseini, H., Niakosari, M., Yousefi, G. H., & Golmakani, M. T. (2016). Physicochemical properties and storage stability of ultrasound-mediated WPI-stabilized fish oil nanoemulsions. *Food Hydrocolloids*, *61*, 801–811. https://doi.org/10.1016/j.foodhyd.2016.07.011

Noronha, C. M., De Carvalho, S. M., Lino, R. C., & Barreto, P. L. M. (2014). Characterization of antioxidant methylcellulose film incorporated with α-tocopherol nanocapsules. *Food Chemistry*, *159*, 529–535. https://doi.org/10.1016/j.foodchem.2014.02.159

Nhan, P. P., & Hoa, N. K. (2013). Effect of Light and Storage Time on Vitamin E in Pharmaceutical Products. *British Journal of Pharmacology and Toxicology*, *4*(5), 176–180. http://maxwellsci.com/print/bjpt/v4-176-180.pdf

Otoni, C. G., Avena-Bustillos, R. J., Olsen, C. W., Bilbao-Sáinz, C., & McHugh, T. H. (2016). Mechanical and water barrier properties of isolated soy protein composite edible films as affected by carvacrol and cinnamaldehyde micro and nanoemulsions. *Food Hydrocolloids*. *57*, 72 - 79. https://doi.org/10.1016/j.foodhyd.2016.01.012

Otoni, C. G., De Moura, M. R., Aouada, F. A., Camilloto, G. P., Cruz, R. S., Lorevice, M. V, Mattoso, L. H. C. (2014). Antimicrobial and physical-mechanical properties of pectin/papaya puree/cinnamaldehyde nanoemulsion edible composite films. https://doi.org/10.1016/j.foodhyd.2014.04.013

Paparella, A., Taccogna, L., Aguzzi, I., Chaves-López, C., Serio, A., Marsilio, F., & Suzzi, G. (2008). Flow cytometric assessment of the antimicrobial activity of essential oils against Listeria monocytogenes. *Food Control*, *19*(12), 1174–1182. https://doi.org/10.1016/j.foodcont.2008.01.002

Peng, Y., & Li, Y. (2014). Combined effects of two kinds of essential oils on physical, mechanical and structural properties of chitosan films. *Food Hydrocolloids*, *36*, 287–293. https://doi.org/10.1016/j.foodhyd.2013.10.013

Pereda, M., Ponce, A. G., Marcovich, N. E., Ruseckaite, R. A., & Martucci, J. F. (2011). Chitosan-gelatin composites and bi-layer films with potential antimicrobial activity. *Food Hydrocolloids*, *25*(5), 1372–1381. https://doi.org/10.1016/j.foodhyd.2011.01.001

Pérez-Córdoba, L. J., & Sobral, P. J. A. (2017). Physical and antioxidant properties of films based on gelatin, gelatin-chitosan or gelatin-sodium caseinate blends loaded with nanoemulsified active compounds. *Journal of Food Engineering*, *213*, 47–53. https://doi.org/10.1016/j.jfoodeng.2017.05.023

Péroval, C., Debeaufort, F., Despré, D., & Voilley, A. (2002). Edible Arabinoxylan-Based Films. 1. Effects of Lipid Type on

873 Water Vapor Permeability, Film Structure, and Other Physical Characteristics. *Journal of Agriculture and Food*
874 *Chemistry*, *50*(14), 3977 – 3983. https://doi.org/10.1021/JF0116449
875 Ponce, A. G., Roura, S. I., del Valle, C. E., & Moreira, M. R. (2008). Antimicrobial and antioxidant activities of edible
876 coatings enriched with natural plant extracts: In vitro and in vivo studies. *Postharvest Biology and Technology*, 49(2),
877 294 - 300. https://doi.org/10.1016/j.postharvbio.2008.02.013
878 Pranoto, Y., Rakshit, S. K., & Salokhe, V. M. (2005). Enhancing antimicrobial activity of chitosan films by incorporating
879 garlic oil, potassium sorbate and nisin. *LWT - Food Science and Technology*, *38*(8), 859–865.
880 https://doi.org/10.1016/j.lwt.2004.09.014
881 Re, R., Pellegrini, N., Proteggente, A., Pannala, A., Yang, M., & Rice-Evans, C. (1999). Antioxidant Activity Applying an
882 Improved Abts Radical Cation Decolorization Assay, *Free radical biology and medicine*, *26*(9-10), 1231–1237.
883 Rhim, J. W., & Ng, P. K. W. (2007). Natural biopolymer-based nanocomposite films for packaging applications. *Critical*
884 *Reviews in Food Science and Nutrition*, *47*(4), 411–433. https://doi.org/10.1080/10408390600846366
885 Rivero, S., García, M. A., & Pinotti, A. (2009). Composite and bi-layer films based on gelatin and chitosan. *Journal of Food*
886 *Engineering*, *90*, 531–539. https://doi.org/10.1016/j.jfoodeng.2008.07.021
887 Rubilar, J. F., Cruz, R. M. S., Silva, H. D., Vicente, A. A., Khmelinskii, I., & Vieira, M. C. (2013). Physico-mechanical
888 properties of chitosan films with carvacrol and grape seed extract. *Journal of Food Engineering*, *115*(4), 466–474.
889 https://doi.org/10.1016/j.jfoodeng.2012.07.009
890 Saberi, A. H., Fang, Y., & McClements, D. J. (2013). Fabrication of vitamin E-enriched nanoemulsions: Factors affecting
891 particle size using spontaneous emulsification. *Journal of Colloid and Interface Science*, *391*(1), 95–102.
892 https://doi.org/10.1016/j.jcis.2012.08.069
893 Salvia-Trujillo, L., Rojas-Graü, M. A., Soliva-Fortuny, R., & Martín-Belloso, O. (2013). Effect of processing parameters on
894 physicochemical characteristics of microfluidized lemongrass essential oil-alginate nanoemulsions. *Food*
895 *Hydrocolloids*, *30*(1), 401–407. https://doi.org/10.1016/j.foodhyd.2012.07.004
896 Sari, T. P., Mann, B., Kumar, R., Singh, R. R. B., Sharma, R., Bhardwaj, M., & Athira, S. (2014). Preparation and
897 characterization of nanoemulsion encapsulating curcumin. *Food Hydrocolloids*, *43*, 540 - 546.
898 https://doi.org/10.1016/j.foodhyd.2014.07.011
899 Sasaki, R. S., Mattoso, L. H. C., & de Moura, M. R. (2016). New Edible Bionanocomposite Prepared by Pectin and Clove
900 Essential Oil Nanoemulsions. *Journal of Nanoscience and Nanotechnology*, *16*(6), 6540–6544.
901 https://doi.org/10.1166/jnn.2016.11702
902 Seydim, A. C., & Sarikus, G. (2006). Antimicrobial activity of whey protein based edible films incorporated with oregano,
903 rosemary and garlic essential oils. *Food Research International*, *39*, 639–644.
904 https://doi.org/10.1016/j.foodres.2006.01.013
905 Soazo, M., Rubiolo, A. C., & Verdini, R. A. (2011). Effect of drying temperature and beeswax content on moisture
906 isotherms of whey protein emulsion film. *Procedia Food Science*, *1*, 210–215.
907 https://doi.org/10.1016/J.profoo.2011.09.033
908 Sobral, P. J. A., Menegalli, F. C., Hubinger, M. D., & Roques, M. A. (2001). Mechanical, water vapor barrier and thermal
909 properties of gelatin based edible films. *Food Hydrocolloids*, *15*(4–6), 423–432. https://doi.org/10.1016/S0268-
910 005X(01)00061-3
911 Statgraphics Centurion XV Software (StatPoint, Inc.), 2006. Version 15.2. 05. Statistical Graphics Corp., Warrenton,
912 Virginia.
913 Sung, S. Y., Sin, L. T., Tee, T. T., Bee, S. T., & Rahmat, A. R. (2014). Effects of Allium sativum essence oil as
914 antimicrobial agent for food packaging plastic film. *Innovative Food Science and Emerging Technologies*, *26*, 406–
915 414. https://doi.org/10.1016/j.ifset.2014.05.009
916 Tan, C. P., & Nakajima, M. (2005). β-Carotene nanodispersions: Preparation, characterization and stability evaluation. *Food*
917 *Chemistry*, *92*, 661–671. https://doi.org/10.1016/j.foodchem.2004.08.044
918 Tongnuanchan, P., Benjakul, S., & Prodpran, T. (2012). Properties and antioxidant activity of fish skin gelatin film
919 incorporated with citrus essential oils. *Food Chemistry*, *134*(3), 1571–1579.
920 https://doi.org/10.1016/j.foodchem.2012.03.094
921 Tongnuanchan, P., Benjakul, S., & Prodpran, T. (2013). Physico-chemical properties, morphology and antioxidant activity
922 of film from fish skin gelatin incorporated with root essential oils. *Journal of Food Engineering*, *117*(3), 350–360.
923 https://doi.org/10.1016/j.jfoodeng.2013.03.005
924 Tongnuanchan, P., Benjakul, S., & Prodpran, T. (2014). Structural , morphological and thermal behaviour characterisations
925 of fi sh gelatin fi lm incorporated with basil and citronella essential oils as affected by surfactants. *Food*
926 *Hydrocolloids*, *41*, 33–43. https://doi.org/10.1016/j.foodhyd.2014.03.015
927 Troncoso, E., Aguilera, J. M., & McClements, D. J. (2012). Fabrication, characterization and lipase digestibility of food-
928 grade nanoemulsions. *Food Hydrocolloids*, *27*(2), 355–363. https://doi.org/10.1016/j.foodhyd.2011.10.014
929 Valencia, G. A., Lourenço, R. V., Bittante, A. M. Q. B., & Sobral, P. J. A. (2016). Physical and morphological properties of
930 nanocomposite films based on gelatin and Laponite. *Applied Clay Science*, *124–125*, 260–266.
931 https://doi.org/10.1016/j.clay.2016.02.023
932 Valenzuela, C., Abugoch, L., & Tapia, C. (2013). Quinoa protein-chitosan-sunflower oil edible film: Mechanical, barrier and
933 structural properties. *LWT - Food Science and Technology*, *50*(2), 531–537. https://doi.org/10.1016/j.lwt.2012.08.010
934 Wang, J., Cao, Y., Sun, B., & Wang, C. (2011). Physicochemical and release characterisation of garlic oil- b -cyclodextrin
935 inclusion complexes. *Food Chemistry*, *127*(4), 1680–1685. https://doi.org/10.1016/j.foodchem.2011.02.036
936 Wayne, P. (2006). Performance Standarts for Antimicrobial Disk Susceptibility Tests; Approved Standard; 9 Edition.
937 Clinical and laboratory standards institute (Vol. 26). http://demo.nextlab.ir/getattachment/27407437-3d73-4048-8239-
938 81857d68cf3d/CLSI-M2-A9.aspx
939 Wei, Q.-Y., Xiong, J.-J., Jiang, H., Zhang, C., & Wen Ye. (2011). The antimicrobial activities of the cinnamaldehyde

adducts with amino acids. *International Journal of Food Microbiology*, *150*(2–3), 164–70. https://doi.org/10.1016/j.ijfoodmicro.2011.07.034

Wu, J., Chen, S., Ge, S., Miao, J., Li, J., & Zhang, Q. (2013). Preparation , properties and antioxidant activity of an active fi lm from silver carp (Hypophthalmichthys molitrix) skin gelatin incorporated with green tea extract. *Food Hydrocolloids*, *32*, 42–51. https://doi.org/10.1016/j.foodhyd.2012.11.029

Yang, Y., & McClements, D. J. (2013). Encapsulation of vitamin E in edible emulsions fabricated using a natural surfactant. *Food Hydrocolloids*, *30*(2), 712–720. https://doi.org/10.1016/j.foodhyd.2012.09.003

Yen, M.-T., Yan, J.-H., & Mau, J.-L. (2008). Antioxidant properties of chitosan from crab shells. *Carbohydrate Polymers*, *74*(4), 840–844. https://doi.org/10.1016/J.CARBPOL.2008.05.003

Yuan, G., Chen, X., & Li, D. (2016). Chitosan films and coatings containing essential oils: The antioxidant and antimicrobial activity, and application in food systems. *Food Research International*, *89*, 117–128. https://doi.org/10.1016/j.foodres.2016.10.004

Figures Captions

Figure 1. Droplet size distributions of O/W nanoemulsions containing encapsulated active compounds as a function of storage time (all systems stored at 4 ºC). **(a)** Control (no encapsulated species); **(b)** α-tocopherol/cinnamaldehyde; **(c)** α-tocopherol/garlic oil; and **(d)** α-tocopherol/ cinnamaldehyde and garlic oil.

Figure 2. (a) 3-D AFM topographic images, and **(b)** profile of the height values along the sample in the marked area of 2D AFM images of O/W nanoemulsions containing encapsulated active compounds. *α-t: α-tocopherol, Cin: cinnamaldehyde, GO: garlic oil.

Figure 3. Diffractograms of gelatin-chitosan films loaded with O/W nanoemulsions containing encapsulated active compounds. N_0 - Control 1: film without nanoemulsion; N_1 - Control 2: film with control nanoemulsion (no encapsulated species); N_2: α-tocopherol/cinnamaldehyde; N_3: α-tocopherol/garlic oil; N_4: α-tocopherol/cinnamaldehyde and garlic oil-loaded nanoemulsion.

Figure 4. DSC thermograms of gelatin-chitosan films loaded with O/W nanoemulsions containing encapsulated active compounds. N_0 - Control 1: film without nanoemulsion; N_1 - Control 2: film with control nanoemulsion (no encapsulated species); N_2: α-tocopherol/cinnamaldehyde; N_3: α-tocopherol/garlic oil; N_4: α-tocopherol/cinnamaldehyde and garlic oil-loaded nanoemulsion. Straight traces correspond to the first scan and broken traces for the second scan.

Figure 5. AFM micrographs of (a) 3D topography and (b) 2D surface of gelatin-chitosan films loaded with O/W nanoemulsions containing encapsulated active compounds. N_0 - Control 1: film without nanoemulsion; N_1 - Control 2: film with control nanoemulsion (no encapsulated species); N_2: α-tocopherol/cinnamaldehyde; N_3: α-tocopherol/garlic oil; N_4: α-tocopherol/cinnamaldehyde and garlic oil-loaded nanoemulsion.

Figure 6. ESEM micrographs of the a) surface and b) cross section of gelatin-chitosan films loaded with O/W nanoemulsions containing encapsulated active compounds. N_0 - Control 1: film without nanoemulsion; N_1 - Control 2: film with control nanoemulsion (no encapsulated species); N_2: α-tocopherol/cinnamaldehyde; N_3: α-tocopherol/garlic oil; N_4: α-tocopherol/cinnamaldehyde and garlic oil-loaded nanoemulsion.

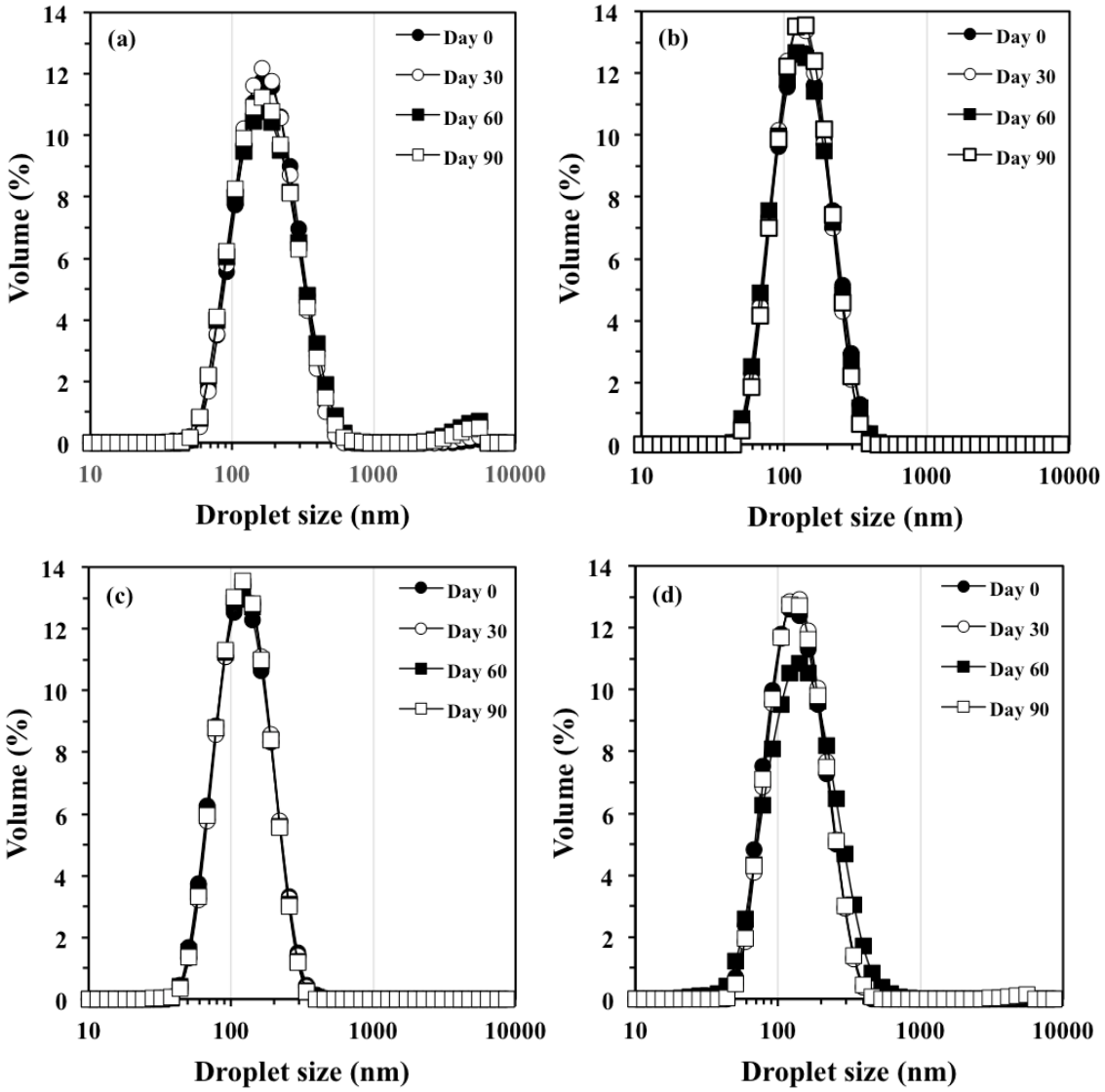

Figure 1. Droplet size distributions of O/W nanoemulsions containing encapsulated active compounds as a function of storage time (all systems stored at 4 ºC). **(a)** Control (no encapsulated species); **(b)** α-tocopherol/cinnamaldehyde; **(c)** α-tocopherol/garlic oil; and **(d)** α-tocopherol/ cinnamaldehyde and garlic oil.

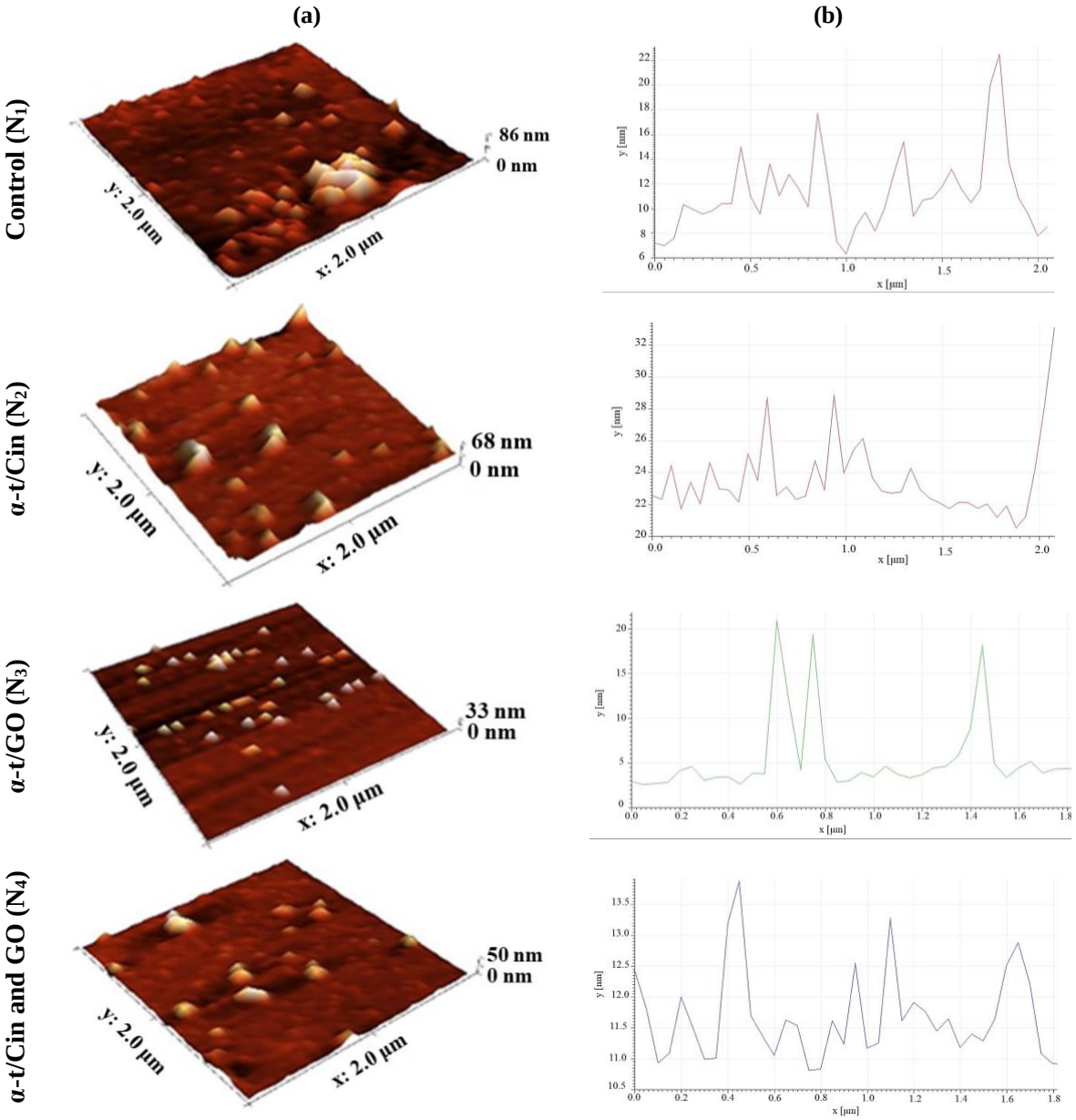

Figure 2. (a) 3-D AFM topographic images, and **(b)** profile of the height values along the sample in the marked area of 2D AFM images of O/W nanoemulsions containing encapsulated active compounds. *α-t: α-tocopherol, Cin: cinnamaldehyde, GO: garlic oil.

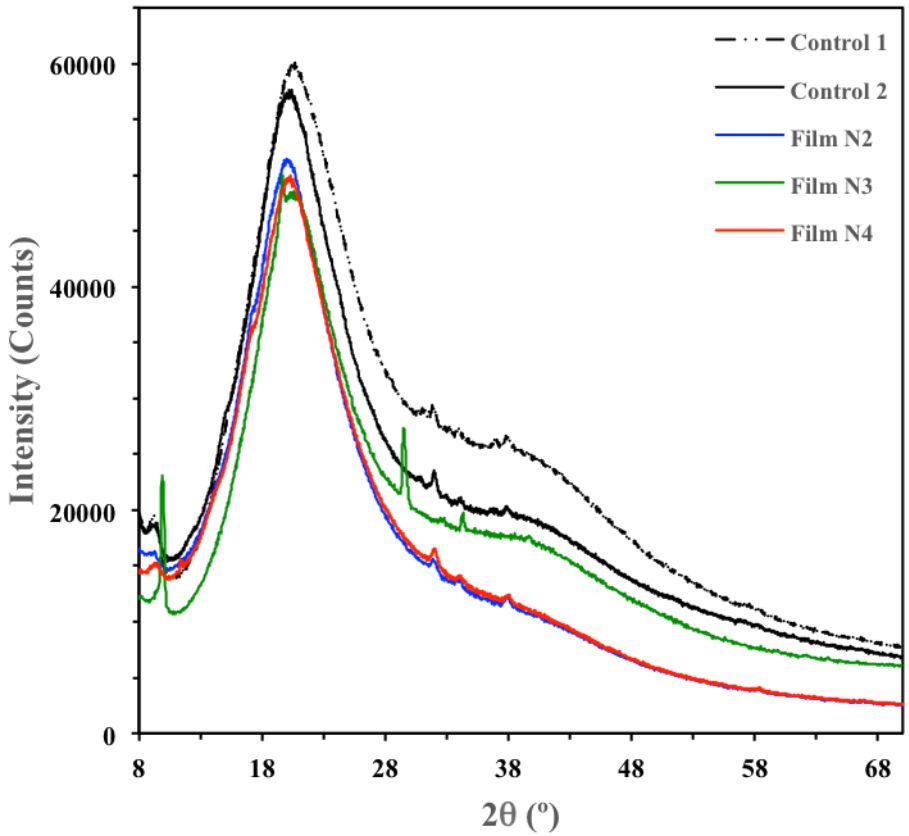

Figure 3. Diffractograms of gelatin-chitosan films loaded with O/W nanoemulsions containing encapsulated active compounds. N_0 - Control 1: film without nanoemulsion; N_1 - Control 2: film with control nanoemulsion (no encapsulated species); N_2: α-tocopherol/cinnamaldehyde; N_3: α-tocopherol/garlic oil; N_4: α-tocopherol/cinnamaldehyde and garlic oil-loaded nanoemulsion.

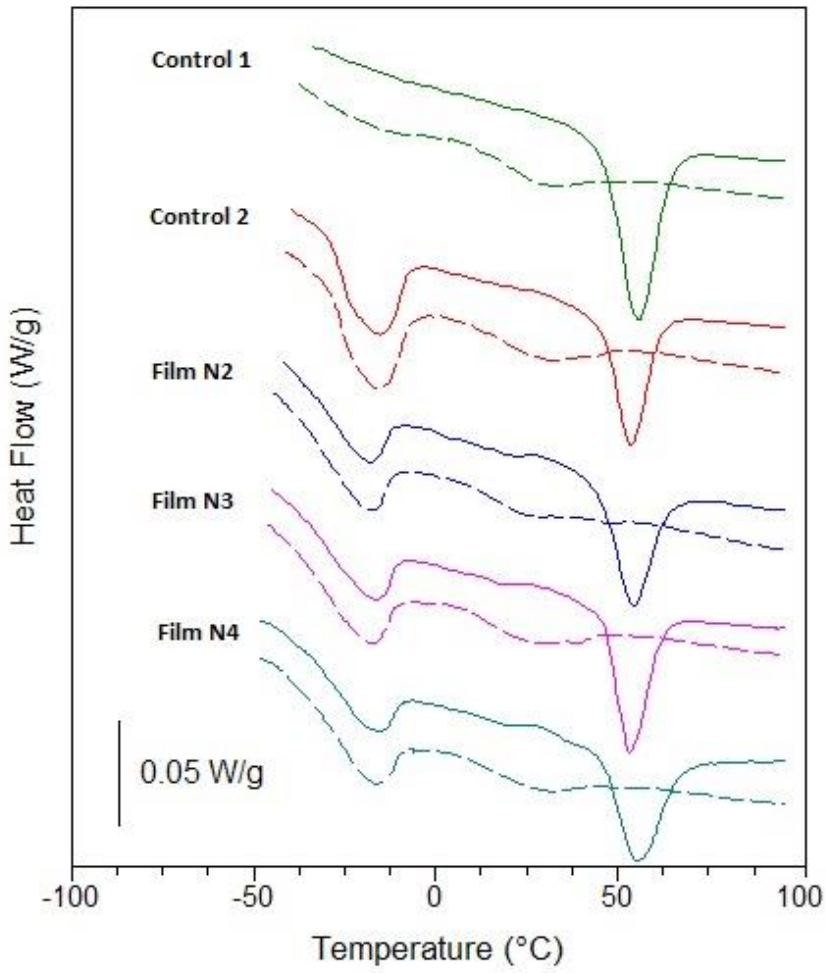

Figure 4. DSC thermograms of gelatin-chitosan films loaded with O/W nanoemulsions containing encapsulated active compounds. N_0 - Control 1: film without nanoemulsion; N_1 - Control 2: film with control nanoemulsion (no encapsulated species); N_2: α-tocopherol/cinnamaldehyde; N_3: α-tocopherol/garlic oil; N_4: α-tocopherol/cinnamaldehyde and garlic oil-loaded nanoemulsion. Straight traces correspond to the first scan and broken traces for the second scan.

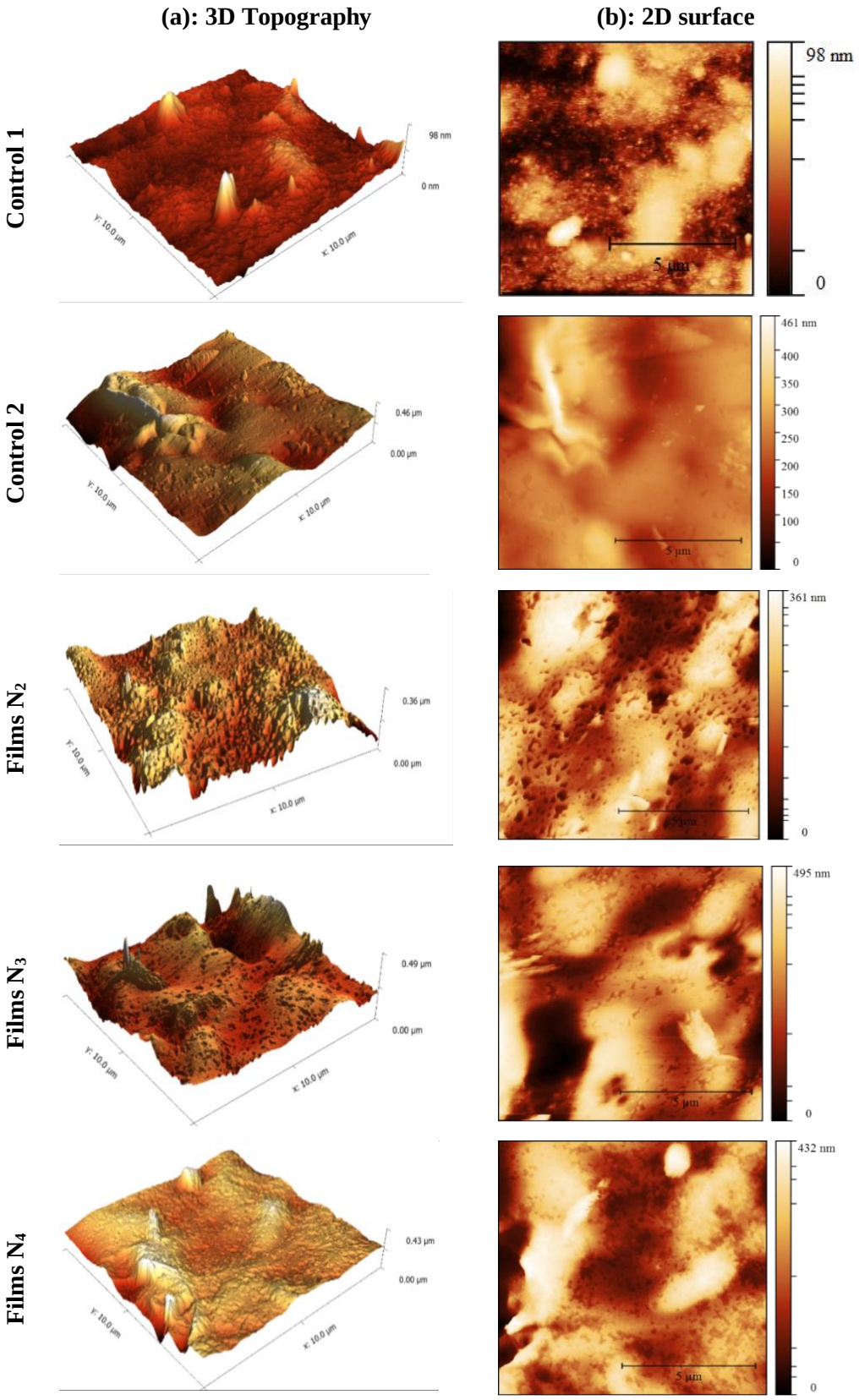

Figure 5. AFM micrographs of (a) 3D topography and (b) 2D surface of gelatin-chitosan films loaded with O/W nanoemulsions containing encapsulated active compounds. N_0 - Control 1: film without nanoemulsion; N_1 - Control 2: film with control nanoemulsion (no encapsulated species); N_2: α-tocopherol/cinnamaldehyde; N_3: α-tocopherol/garlic oil; N_4: α-tocopherol/cinnamaldehyde and garlic oil-loaded nanoemulsion.

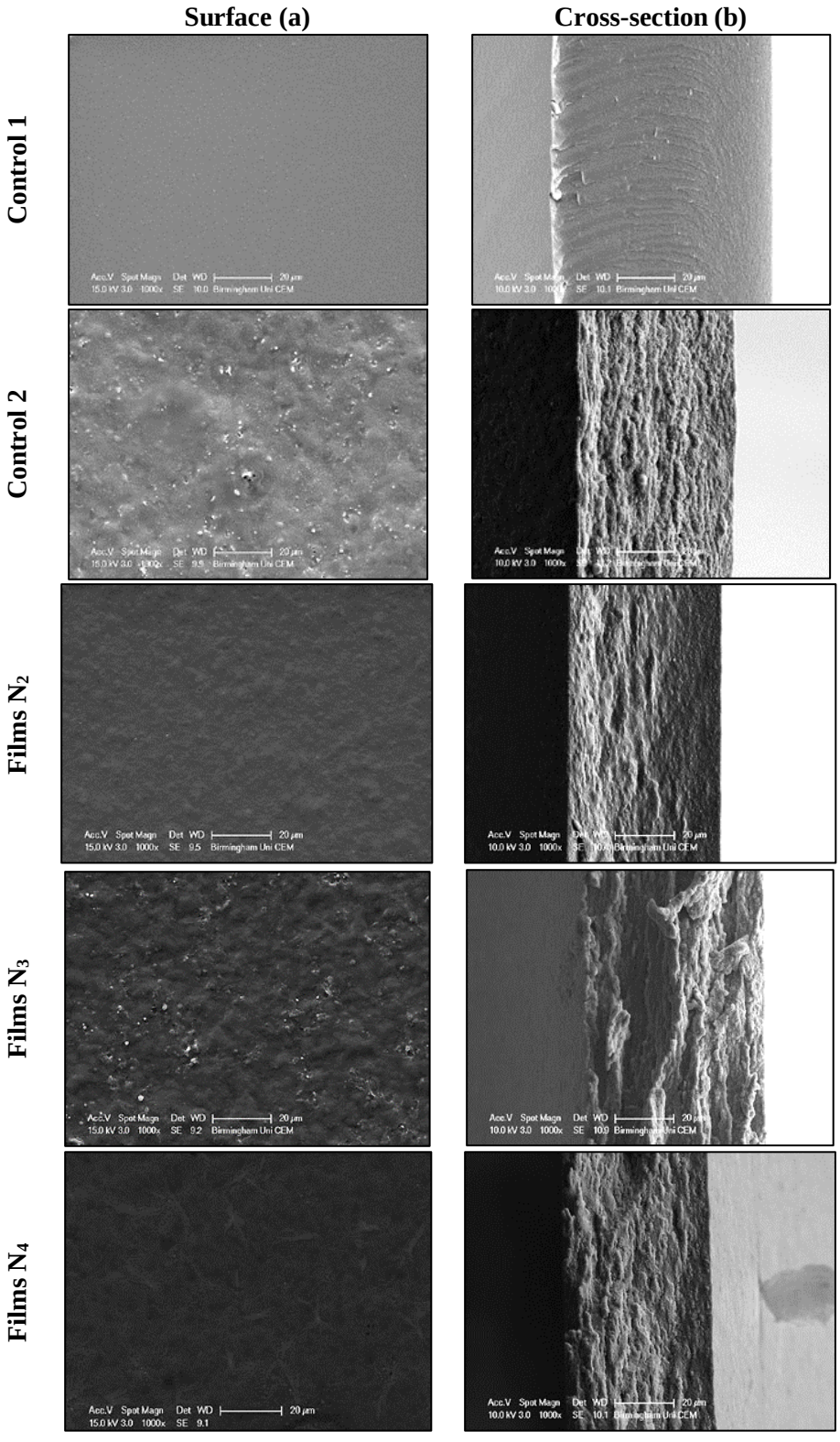

Figure 6. ESEM micrographs of the a) surface and b) cross section of gelatin-chitosan films loaded with O/W nanoemulsions containing encapsulated active compounds. N_0 - Control 1: film without nanoemulsion; N_1 - Control 2: film with control nanoemulsion (no encapsulated species); N_2: α-tocopherol/cinnamaldehyde; N_3: α-tocopherol/garlic oil; N_4: α-tocopherol/cinnamaldehyde and garlic oil-loaded nanoemulsion.

Table 1. Encapsulation efficiencies of cinnamaldehyde, α-tocopherol and garlic oil and mean droplet sizes, polydispersity indices (PDI), ζ-potential and pH values of the O/W nanoemulsions containing these encapsulated active compounds, as a function of storage time (all systems stored at 4±1ºC) .

Samples*	Time (Days)	Encapsulation efficiency			Droplet size (nm)	PDI	ζ-potential (mV)	pH
		Cinnamaldehyde (%)	α-tocopherol(%)	GO(%)				
Control (N_1)	0	----	---	----	157.0 ± 4.1^{aA}	0.19 ± 0.02^{bA}	-17.3 ± 0.6^{aA}	6.1 ± 0.0^{abA}
	30	----	---	----	158.2 ± 2.9^{aA}	0.20 ± 0.02^{bA}	-16.0 ± 1.4^{bA}	6.0 ± 0.0^{bcA}
	60	----	---	----	161.2 ± 5.9^{aA}	0.23 ± 0.02^{aA}	-17.2 ± 0.9^{abA}	6.1 ± 0.0^{aA}
	90	----	---	----	156.9 ± 4.7^{aA}	0.21 ± 0.02^{bA}	-18.1 ± 1.0^{aA}	6.0 ± 0.0^{cA}
α-t/Cin (N_2)	0	100 ± 0.0^{aA}	57.1 ± 1.1^{aA}	----	123.1 ± 1.5^{aB}	0.16 ± 0.01^{aB}	-14.2 ± 0.5^{aC}	5.3 ± 0.0^{aD}
	30	----	---	----	121.5 ± 0.6^{aC}	0.16 ± 0.04^{aB}	-12.3 ± 0.3^{bC}	5.1 ± 0.0^{bC}
	60	----	---	----	121.9 ± 2.7^{aC}	0.15 ± 0.01^{aB}	-13.7 ± 0.9^{aC}	4.7 ± 0.1^{cC}
	90	99.7 ± 0.3^{aA}	46.6 ± 0.4^{bB}		122.4 ± 2.5^{aC}	0.15 ± 0.01^{aBC}	-13.7 ± 1.0^{aC}	4.6 ± 0.0^{dB}
α-t/GO (N_3)	0	----	52.4 ± 0.4^{aA}	92.2 ± 1.9^{aA}	111.0 ± 2.0^{aC}	0.16 ± 0.0^{aB}	-15.9 ± 0.7^{abB}	6.0 ± 0.0^{aB}
	30	----	---	---	112.5 ± 2.4^{aD}	0.14 ± 0.02^{aB}	-15.5 ± 0.6^{abA}	5.4 ± 0.0^{bB}
	60	----	---	---	111.2 ± 1.9^{aD}	0.14 ± 0.01^{aB}	-16.0 ± 0.8^{aB}	4.9 ± 0.0^{cB}
	90	----	47.8 ± 0.2^{bA}	88.5 ± 2.7^{aA}	111.5 ± 1.9^{aD}	0.14 ± 0.01^{aC}	-15.0 ± 0.9^{bB}	4.3 ± 0.0^{dD}
α-t/Cin and GO (N_4)	0	93.9 ± 2.6^{aA}	56.7 ± 3.1^{aA}	70.9 ± 2.0^{aB}	124.8 ± 1.4^{bB}	0.15 ± 0.01^{bB}	-14.4 ± 0.7^{aC}	5.5 ± 0.0^{aC}
	30	---	---	---	126.4 ± 2.2^{bB}	0.16 ± 0.02^{bB}	-13.7 ± 0.4^{bB}	4.9 ± 0.0^{bD}
	60	---	---	---	130.0 ± 1.1^{aB}	0.20 ± 0.01^{aC}	-13.8 ± 0.5^{abC}	4.7 ± 0.0^{cC}
	90	89.6 ± 0.6^{aB}	45.2 ± 0.3^{bC}	61.6 ± 0.1^{bB}	126.6 ± 3.0^{bB}	0.16 ± 0.02^{bB}	-14.5 ± 0.6^{aBC}	4.5 ± 0.0^{dC}

Mean values ± standard deviation (n = 3). Different lower case letters in the same column indicate significant differences ($p<0.05$) for the same sample over different days and different capital letters indicate significant differences ($p<0.05$) among different samples measured at the same time interval (day).
Cin: cinnamaldehyde; α-t: α-tocopherol; GO: garlic oil.
*N_1 : Control nanoemulsion (no encapsulated species); N_2: α-tocopherol/cinnamaldehyde; N_3: α-tocopherol/garlic oil; N_4: α-tocopherol/cinnamaldehyde and garlic oil-loaded nanoemulsion.

Table 2. Physical/Mechanical properties of gelatin-chitosan films loaded with O/W nanoemulsions containing encapsulated active compounds.

Sample *	Thickness (mm)	Moisture content (%)	Solubility in water (%)	Swelling (g/g)	TS (MPa)	EB (%)	EM (MPa)
Films N_0	0.082 ± 0.001^{a}	18.2 ± 0.8^{a}	50.8 ± 0.7^{a}	26.9 ± 2.8^{b}	19.0 ± 2.1^{a}	89.1 ± 6.4^{d}	101.4 ± 4.5^{a}
Films N_1	0.081 ± 0.002^{a}	17.8 ± 1.8^{a}	47.5 ± 0.6^{b}	30.6 ± 0.6^{a}	10.0 ± 1.1^{bc}	123.3 ± 1.3^{a}	29.0 ± 3.6^{c}
Films N_2	0.081 ± 0.002^{a}	18.2 ± 1.8^{a}	44.0 ± 2.1^{c}	27.4 ± 2.5^{ab}	11.4 ± 1.0^{b}	108.7 ± 2.2^{c}	37.3 ± 2.5^{b}
Films N_3	0.081 ± 0.002^{a}	17.3 ± 2.1^{a}	43.1 ± 2.3^{c}	30.3 ± 1.5^{a}	8.9 ± 0.9^{c}	111.7 ± 4.8^{bc}	30.1 ± 4.9^{c}
Films N_4	0.082 ± 0.001^{a}	18.1 ± 2.0^{a}	48.9 ± 0.9^{ab}	25.3 ± 0.8^{b}	9.8 ± 3.7^{bc}	113.2 ± 2.1^{b}	39.2 ± 3.6^{b}

Mean values ± standard deviation (n = 3). Different letters in the same column indicate significant differences ($p<0.05$).
* N_0 - *Control 1:* film without nanoemulsion; N_1 - *Control 2:* film with control nanoemulsion (no encapsulated species); N_2: α-tocopherol/cinnamaldehyde; N_3: α-tocopherol/garlic oil; N_4: α-tocopherol/cinnamaldehyde and garlic oil-loaded nanoemulsion.
TS: Tensile strength; EB: Elongation at break; EM: Elastic modulus.

Table 3. Light transmittance (%) and transparency of gelatin-chitosan films loaded with O/W nanoemulsions containing encapsulated active compounds.

	Light transmittance (%)						
	Wavelength (nm)						**Transparency**
Sample*	**250**	**280**	**350**	**450**	**600**	**800**	**value**
Films N_0	22.2 ± 0.3^{a}	23.9 ± 0.6^{a}	80.0 ± 0.4^{a}	90.9 ± 0.2^{a}	94.7 ± 0.2^{a}	97.6 ± 0.2^{a}	0.29 ± 0.01^{e}
Films N_1	5.0 ± 0.7^{b}	9.6 ± 0.3^{b}	66.3 ± 0.7^{bc}	77.6 ± 0.5^{d}	83.7 ± 0.4^{d}	88.8 ± 0.4^{e}	0.96 ± 0.02^{a}
Films N_2	0.0 ± 0.0^{c}	0.1 ± 0.0^{d}	63.7 ± 1.4^{d}	85.7 ± 0.6^{b}	91.4 ± 0.4^{b}	95.4 ± 0.4^{b}	0.48 ± 0.02^{d}
Films N_3	0.1 ± 0.0^{c}	0.7 ± 0.0^{c}	67.5 ± 1.7^{b}	83.8 ± 1.7^{c}	87.7 ± 1.4^{c}	91.2 ± 1.4^{d}	0.71 ± 0.09^{b}
Films N_4	0.0 ± 0.0^{c}	0.1 ± 0.0^{d}	65.0 ± 1.0^{cd}	84.5 ± 0.6^{bc}	88.9 ± 0.5^{c}	92.5 ± 0.6^{c}	0.63 ± 0.03^{c}

Mean values ± standard deviation (n = 3). Different letters in the same column indicate significant differences ($p<0.05$).
* N_0 - *Control 1:* film without nanoemulsion; N_1 - *Control 2:* film with control nanoemulsion (no encapsulated species); N_2: α-tocopherol/cinnamaldehyde; N_3: α-tocopherol/garlic oil; N_4: α-tocopherol/cinnamaldehyde and garlic oil-loaded nanoemulsion.

Table 4. Thermal properties and roughness characteristics of gelatin-chitosan films loaded with O/W nanoemulsions containing encapsulated active compounds.

	1st Scan			2nd Scan	Roughness	
Sample*	**T_g (ºC)**	**ΔH_g (J/g)**	**T_m (ºC)**	**T_g (ºC)**	**R_a (nm)**	**R_q (nm)**
Films N_0	45.6 ± 0.6^a	12.1 ± 0.8^b	54.9 ± 0.8^a	8.6 ± 2.2^{ab}	7.5	11.1
Films N_1	46.2 ± 0.8^a	9.3 ± 0.9^a	53.5 ± 0.2^a	12.1 ± 1.1^a	44.1	58.6
Films N_2	45.5 ± 0.4^a	9.0 ± 0.2^a	54.4 ± 0.2^a	8.2 ± 2.7^{ab}	31.4	40.5
Films N_3	46.6 ± 2.3^a	9.6 ± 0.8^a	56.6 ± 5.2^a	10.4 ± 3.1^{ab}	39.5	53.9
Films N_4	45.6 ± 0.4^a	9.3 ± 0.5^a	54.6 ± 0.2^a	6.7 ± 1.4^b	32.3	42.6

Mean values ± standard deviation (n = 3). Different letters in the same column indicate significant differences ($p<0.05$).

* N_0 - *Control 1:* film without nanoemulsion; N_1 - *Control 2:* film with control nanoemulsion (no encapsulated species); N_2: α-tocopherol/cinnamaldehyde; N_3: α-tocopherol/garlic oil; N_4: α-tocopherol/cinnamaldehyde and garlic oil-loaded nanoemulsion.

T_g: Glass transition temperature; T_m: Melting temperature; ΔH_g: Melting enthalpy; R_a: average roughness; R_q: root-mean-square roughness.

Table 5. Inhibition halos against *P. aeruginosa* and *L. monocytogenes* and Trolox Equivalent Antioxidant Capacity (TEAC) of gelatin-chitosan films loaded with O/W nanoemulsions containing encapsulated active compounds.

Sample*	Zone of inhibition (mm^2)		**TEAC (µmol TE/g dried film)**		
	P. aeruginosa	***L. monocytogenes***	**DPPH• method**	**ABTS•+ method**	**FRAP assay**
Films N_0	0.0 ± 0.0^{c}	0.0 ± 0.0^{a}	0.0 ± 0.0^{c}	0.0 ± 0.0^{d}	6.9 ± 0.4^{e}
Films N_1	0.0 ± 0.0^{c}	0.0 ± 0.0^{a}	0.0 ± 0.0^{c}	1.3 ± 0.0^{c}	39.8 ± 0.2^{d}
Films N_2	138.2 ± 2.4^{a}	0.0 ± 0.0^{a}	0.2 ± 0.0^{a}	2.6 ± 0.1^{a}	49.9 ± 1.2^{c}
Films N_3	138.2 ± 0.0^{a}	0.0 ± 0.0^{a}	0.1 ± 0.0^{b}	2.5 ± 0.0^{a}	81.5 ± 2.2^{a}
Films N_4	65.4 ± 1.4^{b}	0.0 ± 0.0^{a}	0.1 ± 0.0^{b}	2.3 ± 0.1^{b}	68.3 ± 2.9^{b}

Mean values ± standard deviation (n = 3). Different letters in the same column indicate significant differences ($p<0.05$).
* N_0 - *Control 1:* film without nanoemulsion; N_1 - *Control 2:* film with control nanoemulsion (no encapsulated species); N_2: α-tocopherol/cinnamaldehyde; N_3: α-tocopherol/garlic oil; N_4: α-tocopherol/cinnamaldehyde and garlic oil-loaded nanoemulsion.